**Reviewer #1**

The paper is reasonable as a description of a retrieval method, but it lack a demonstration that the algorithm is practically useful. The authors present the evaluation of simulated data, but do so in such idealised circumstances that the exercise provides little insight into the algorithm's overall utility. However, the presentation is decent and the central idea interesting and worth publishing, even if I'm not entirely convinced it is valid.

The paper presents a new concept for the retrieval of aerosol single scattering properties that have never been published before. As this concept is new, it has been presented in ideal situation to ease its understanding.

To be more specific in my critique:
• The paper must demonstrate the algorithm applied to noisy data. As it stands, the results shown are somewhat concerning as the algorithm can only precisely replicate the truth in the simplest case despite perfect input data. This implies significant (if not large) forward model errors that the paper neither discusses, quantifies, nor attempts to alleviate. Considering CISAR has already been applied to real data, this demonstration should be a straightforward matter of adding random noise to the existing experiment's data and adding an additional line to Figs. 5–9 for the retrieval under noise.

Adding noise to the simulated data is certainly useful as actual observations are not noise free. However, in that case, the performance of the method would need to be statistically demonstrated applying the retrieval on a large number of simulations. We do not believe that it would have ease the reading of the results. Similarly to adding noise to the data, we would have to consider actual observation conditions and include sections on information content specific to the selected radiometer and orbit. In order to avoid all these considerations and keep focused on the actual paper objective, we prefer not to start addressing these practical issues in this theoretical paper.

The following sentence has been added at the end of Section 4.4

A similar comparison has been performed against actual PROBA-V observations (Luffarelli et al., 2017). These comparisons a root mean square error between simulated and actual observations of about 0.03.

The following sentence has been added to Section 6.1, experimental setup.

An uncertainty of 3% is assumed in matrix S_y.

• Additionally, your experiments assume that the surface parameters are known a priori. That is unacceptable considering the title of the paper is 'joint retrieval of surface reflectance and aerosol properties'. If you promise a joint retrieval, you need to demonstrate it. If you don't intend to demonstrate it, redraft the paper to de-emphasise the surface terms while explaining why you built a joint retrieval and chose not to use it. Such a demonstration is important as the reader needs to understand how the optimal estimation balances uncertainties in aerosol against the surface. (I would show averaging kernels, but that isn't widely popular.)

This specific issue of surface retrieval has been addressed in a previous paper by Wagner et al. (2010). This paper demonstrates that an accurate retrieval of surface reflectance is

possible with this joint retrieval approach. It requires however to include a complex scheme for the estimation of the surface prior information from the previous retrieval. Once again, we prefer to avoid these aspects as there were already published and deviate from the paper primary objective.

• From my experience teaching linear algebra, I would summarise the paper's central idea as, "Rather than assume aerosol optical properties for the retrieval, one should define a basis of aerosol types. The observed properties of any real aerosol are then some linear combination of the properties of those basis types."

This statement correctly summarizes the paper concept. However, the possibility to express the scattering albedo and phase function values as a linear mixture of the vertices properties need to be demonstrated. That is the main purpose of Section 6. The end of Section 1 has been re-written and reads now

The advantages of a continuous variation of the aerosol properties in the solution space against a LUT-based approach is discussed in Section (3). The proposed method expresses the scattering albedo and phase function values as a linear mixture of basic aerosol classes. The forward radiative transfer model that includes the Jacobians computation is described in Section (4). With the exception of gaseous transmittance, this model no longer relies on LUTs, and the RTE is explicitly solved. The inversion method is described in Section (5). Finally, the possibility to express aerosol single scattering properties as a linear combination is illustrated with simulated data representing various scenarios including small and large particles (6).

From that, I wonder if you could use an objective technique to select your vertices? Given that a large number of aerosol types are currently defined, there are various techniques within linear algebra from which a minimal set of types can be derived (e.g. Gram-Schmidt or one of the eigenfunction analyses). This could give you better fits in the ideal circumstances and would unambiguously resolve the question of how many vertices you should use (which is rather unsatisfying at the moment).

Please refer to our answer of Reviewer #2 main concern.

• A central assumption of the paper is that either the surface or the aerosol vary sufficiently slowly as to be effectively constant over the observation period. There needs to be some justification of this. I wouldn't accept a simple citation of existing work as the quality of such assumptions is highly dependent on exactly where and how you evaluate them.

This comment is fully justified. The speed at which surface radiative properties changes is also highly dependent on the spatial resolution. This method has been published in JGR and we do not see the need to come back on that work. It allows to stay focused on the paper objective. We however allow the aerosol optical thickness to vary quite rapidly.

• Various sections of this paper rely on a familiarity with Govaerts et al. (2010). A less brief summary of it's conclusions and how that method differs from this one would be useful to the casual reader.

The two main differences between Govaerts et al. (2010) and the current version are listed in Section 2. It concerns:

- The retrieval is not performed any more for a limited number of prescribed aerosol classes but with a continuous sampling of the solution space bounded by the vertices;
- The forward model solutions are not pre-calculated for a limited number of solutions and stored in LUTs. In this new model, the radiative transfer equation is solved online. It allows calculating the derivatives in any points of the solution space. With a LUT-based approach, it is also possible but very CPU intensive.

L95 While it is strictly true that optimal estimation requires state vector variables to be continuous, I feel that your argument here mis-characterises what is going on. As you admit, there are over 100 variables that affect the radiance seen at TOA scattered by aerosols. The prevalent approach is to assume that most of those variables are determined at the aerosol's creation. Diner et al. (2012) demonstrated that superior results can be obtained by assuming less when additional information is available (specifically, multi-angular observations).
To me, it seems obvious that attempting to retrieve either more variables or more physically motivated variables will result in a higher quality retrieval. The issue isn't that most retrievals assume an aerosol type. Their issue is that they use too few observations to assume anything better. To put it differently, your retrieval is superior because it uses more data and so can vary more variables, providing the OE algorithm with more freedom to find an accurate solution.

As explained in Section 2, there is an inconstancy in trying to apply an OE approach and the use of pre-defined aerosol classes. By doing so, it is assumed that the solution should precisely correspond to these classes. It imposes thus very strong prior information on aerosol single scattering properties. However, there is no uncertainty associated to this prior information, which is inconsistent. Secondly, in order to find the minimum of the cost function, the derivatives of all state variables should be defined in any points of the solution space. This is clearly not the case with the use of pre-defined aerosol classes. The method proposed here addresses specifically this limitation.

L 202 I have a problem with your terminology here. My experience is that in aerosol remote sensing 'single' or 'multiple' refers to the number of times that the light is scattered by an aerosol particle. Eq. (2) quantifies the reflection from the surface.

It also refers to the possible interaction with the surface not only aerosols.

I would like to see a justification for this other than 'it works in Sec. 6.' Firstly, I'm uncertain if you are only considering single aerosol scattering or not. While I'm quite happy that single-scatting properties combine linearly, I am suspicious of this being true for multiple-scattering. Secondly, I doubt that linearity would hold for large optical depths. I expect that your technique is a reasonable approximation, but you should directly assess the error introduced (i.e. don't just work it out after-the-fact from the quality of your retrievals).

Forward and backward simulation are calculated accounting for the multiple scattering contribution as can be seen in Eq. (1) term $\mathrm{I_m}^{\uparrow}$ .

The linear approximation used to express aerosol single scattering properties has no influence on the way the multiple scattering contribution is calculated. No linear approximation is performed on the estimation of $\mathrm{I_m}^{\uparrow}$whatherever the optical thickness.

Tab 1. Are these values ever used within the retrieval to represent forward model error? If not, they should be.

Yes, there are. The following sentence has been added at the end of Section 4.4

A similar comparison has been performed against actual PROBA-V observations (Luffarelli et al., 2017). These comparisons a root mean square error between simulated and actual observations of about 0.03.

The following sentence has been added to Section 6.1, experimental setup.

An uncertainty of 3% is assumed in matrix S_y.

L314 I have no problem citing grey literature in general, but this is unacceptable. The context implied to me that this referred to a validation study, not an unreviewed conference poster. I assume that application of CISAR to real data is in Part 2 (which really should have been submitted alongside this paper) and this reference should be adjusted accordingly.

We acknowledge that the part 2 should have been ready at the same time of part 2. Unfortunately it has not been possible. We will now submit this part in the coming weeks.

L402 This paper contains no analysis of other OE techniques. You cite other studies, but they only comment on specific algorithms. I have no problem with the conclusion that retrieving SSA and phase function provides 'better' results than not doing that when multi-angular observations are available. Your use of multiple MODIS overpasses to emulate multi-angular observations is fine only in those parts of the world where the aerosol or surface is constant over a period of days. Those of us evaluating plumes or areas that suffer frequent cloud cover can't make that assumption and your rejection of such work is excessive.

Aerosols do not require to be constant during the retrieval in case data are accumulated over time to form a multi-angular vector. Only the surface radiative properties are assumed to be invariant. An example of AOT hourly retrieval from SEVIRI can be found in Luffarelli et al., (2016). Example of plume retrieval over bright surface can be found here : http://www.rayference.eu/1/cisar_seviri.php. Example of retrieval for polar orbiting instrument can be found in Luffarelli et al., 2017.

L425 Experiment F00 did not prove your assumptions are valid. It showed that they might work in one circumstance, and even if you had made a comprehensive evaluation I'd say you only showed that the assumptions were 'useful'. I might accept 'Experiment F00 demonstrated that such assumptions can produce accurate retrievals.' However, my earlier concern that your experiments are insufficient to demonstrate the utility of your method remains.

This result is fundamental as it demonstrates the possibility to express the aerosol single scattering properties with Eq. (8) and (9) in inverse mode. This demonstration has been initiated with a simple case and which is further elaborated throughout the experiments.

L433 This statement is far too broad. Replace 'which provide a limited number of independent observations' with something that expresses the limitation of your technique. As it stands, it reads like your algorithm could use any input data and that is plainly false.

This sentence has been deleted and will be moved in Part 2 of the manuscript.

L435 I agree that the choice of vertices is critical. Your empirical selection is unsatisfying and this choice needs more thorough consideration.

Please refer to the reply of Review #2 main comment.

• I have several issues with the title.
– Though the algorithm can technically retrieve surface properties, this is not demonstrated in the paper nor really discussed other than as a component of an aerosol retrieval. The author's previous paper discussed the surface at great length and, though I don't expect them to replicate that here, a paper on a 'joint retrieval of surface reflectance and aerosol properties' should discuss and demonstrate both.

This part will be specifically demonstrated in part 2. There is nothing really new or original concerning the theoretical aspects of the surface property retrieval in this paper with respect to our previously published results. It is the reasons why we did not elaborate these aspects in this theoretical paper. What we clearly stressed in Section 2 is the importance of jointly retrieved surface and aerosol properties as they are the corresponding radiative fields are tightly coupled.

– The authors rightly wish to highlight the unique consideration of multiple types within their retrieval. However, 'continuous variations of the state variables in solution space' fails at that. At first glance, the phrase was virtually meaningless as optimal estimation can only be applied to continuous variables. What the authors have done is define state space differently, such that the retrieval can consider variations along different axes. As an alternatives, I recommend 'Retrieval of surface reflectance and aerosol optical properties through decomposition into representative types: Part 1: theory' or 'Retrieval of surface reflectance and aerosol optical properties by simultaneously considering a representative set of aerosol types: Part 1: theory'.

This remark is too obscure for me to be able to comment it.

– Regardless, 'variations' should be singular.

This typo has been corrected.

L98 Though MISR might not assign uncertainty to aerosol class, that doesn't mean you can't and that people haven't.

The sentence is written in the context of estimating retrieval uncertainty in an OE context as described in Rodger (2000).

L171 Are you sure Liu and Ruprecht (1996) is the most appropriate reference for your radiative transfer solver? That paper assumed spheres and spends a lot of time talking about the microwave.

Yes, the reference is the correct one, being referred to the Matrix Operator Method.

L207 Why use finite differences to calculate the Jacobian? It's slow and inaccurate while all the solvers I know provide analytic Jacobians nowadays. If your solver doesn't provide them,

you should explore alternatives. My experience is that the discontinuities produced by finite differences make optimal estimation much more sensitive to the first guess and take longer to converge.

It would be so nice to have an analytic solution of the multiple scattering equation. Unfortunately, it is not the case.

p10 L3 Shouldn't the phase function be a function of angle too?

The typo has been corrected.

Eq.(8) Is $\tau$ a that defined in Eq. (3) or should it be an equivalent definition using $\tau'$ ?

This typo has been corrected.

L220 A superior sentence would be, "The relative RMSE between FASTRE and the reference model is in the range 1 – 3%." There's no need to hide the larger difference in the 0.44 channel.

The text has been corrected accordingly.

Eq. (11) The third and fourth terms are common, but they aren't from Rodgers (2000). You'll need another reference for them.

The following reference has been added: Dubovik et al., (2011)

Tab. 2 Why doesn't F0 have a value for Nf ?

These types are mono-modal.

L328 Delete the sentence starting 'The estimated single scattering. . . "

For which reason should we delete this sentence?

Sec 6.1 Precisely how many observations are you using and what instrument are you emulating?

We are not simulating a specific instrument. Observations are simulated in the principal plane every 5 degrees.

The following recommendations have been implemented in the text:

L22 In most of the cases an increase
L23 for an increase of in the fraction
L25 does not allow to full characterisation of the underlying
L35 product generation from archived
L54 Such an approach prevents
L74 that time in the EUMETSAT
L77 to 1. It This represents a severe limitation
L78 exceed such a limit.
L83 initiative to generate for a Climate Data Record (CDR) generation of

L91 coupling with the atmospheric scattering
L98 are defined as a prior knowledge
L105 considerable amount number of observations, such as those
L109 a large amount number of observations
L114 easily applied on to observations
L121 should actually only be applied on to the entire phase function Φ only. These
L131 Errant space after 'distribution'
L133 vary essentially mostly as a
L175 computes separately the contributions from single and multiple scattering separately, the
L194 represented by an external
Fig4 radiatively coupled with the
p10 L4 These The different vertices, representing fine and coarse mode aerosols, are
L219 As can be seen, in most of the bands the relative
L230 where most likely the atmospheric properties likely remain unchanged
L238 which increases the number
L241 thickness $\tau_v$ of for the respective aerosol vertices that are mixed in layer $L_a$ used. Prior information
L242 consists of expected values $x_b$ of the state variables $x_b$ characterising
L243 regularization on of the spectral
L247 will be further herein referred to
L279 state variables, such as the
L280 weight, etc, are
L317 showing thereby therefore that the
L321 differs from the ones of these
L323 wavelength is actually limited
L332 as the straight difference
L351 Units shouldn't be italicised.
L377 The errors $\varepsilon_\tau$ is in this experiment F12 are further reduced with respect compared to
L378 manages however to
L405 allowing a continuous variation
L406 having the parameters describing the aerosol
L480 This reference is missing the page number. Also, the DOI has a space in it for some reason.
L512 This DOI also has a space.

**Reviewer #2**

The manuscript fails in providing the most interesting piece of information, i.e. HOW to choose the set of vertices for each operational inversion.

There are several ways to determine the location of the aerosol vertices. One possibility is to look at the Fig. 3 has been modified. This Figure shows a density plot of the ssa – asymmetry factor derived from AERONET observations in the blue band. Such type of information can be used to adjust the location of the vertices. The following text has been added to the manuscript:
The actual extent of possible solutions in the [g,ω0] space for a given spectral band can be outlined by a series of vertices characterizing aerosol single scattering properties. Following Fig. (2), these vertices are defined by an absorbing and a non-absorbing fine mono-mode classes with a small radius, labelled respectively FA and FN and by two coarse mono-modes with different radii, *i.e.*, large and small, labelled respectively CL and CS. Such vertices define a polygon within the [g,ω0] solution space (Fig. 3). The number of vertices can be adjusted according to the amount of spectral observations and expected type of aerosols. In Section (4), we will see how any pair of single scattering albedo and phase function values in that space can be expressed as a linear combination of the vertex properties. The choice of these vertices is critical as they should encompass all possible aerosol single scattering properties that could be observed at a given time and location. Different approaches could be used to define the position of these vertices. These positions could be derived from the analysis of typical aerosol single scattering properties available in databases such as Optical Properties of Aerosols and Clouds (OPAC) (Hess et al., 1998). Alternatively, it is also possible to follow a similar approach as the one proposed in Govaerts et al. (2010) who analysed the single scattering albedo and phase function values derived from AERONET observations acquired in a specific region of interest for a given period (Dubovik et al., 2006). Fig. (3) shows an example of such type of analysis performed in the blue spectral region. The red isoline on that Fig. delineates the area of the [g,ω0] space where 99.7% of the aerosol single scattering properties derived by Dubovik et al. (2006) from AERONET observations are located. The green and blue lines show respectively the 95% and 68% probability regions. These values have been derived using all available Level 2 AERONET observations since 1993. Finally, the model proposed by Schuster et al. (2005) can be used to determine the spectral variations of the single scattering properties outside the spectral bands measured by AERONET. The present study relies on simulated data and the aerosol vertices have been positioned to sample the solution space in a realistic way. In case of the processing of actual satellite data over a specific region or period, it is advised to calculate the isolines corresponding to that region of interest and to adjust the position of the aerosol vertices accordingly.

- Major concerns remain towards the real applicability of this inversion given the highly idealized choice of parameters and observation scenario (rather atypical of satellite observations). It's OK to make this the first part of a dual-paper study, but at this point the two manuscripts should be submitted together so that the reviewers could be convinced of the ultimate and general performance of the method. I have looked into http://www.rayference.eu/CISAR/SEVIRI_report.pdf as suggested in the authors' preliminary response, yet that report deals with only one study case where the conclusion seems to be that the AOT is systematically underestimated (by ~50%!) with respect to AERONET observations (it is of course possible I'm missing something).

This report contains the analysis of a very limited number of aerosol stations. The following Figure taken from Luffarelli, M., Y. Govaerts, and C. Goossens. 2017. 'Joint Retrieval Of

Surface Reflectance And Aerosol Properties: Application To MSG/SEVIRI in the Framework of the Aerosol_cci Project'. In *EGU General Assembly Conference Abstracts*, 19:5398. EGU General Assembly Conference Abstracts and have been derived over a large number of AERONET stations. These results will be published in the second part of this manuscript.

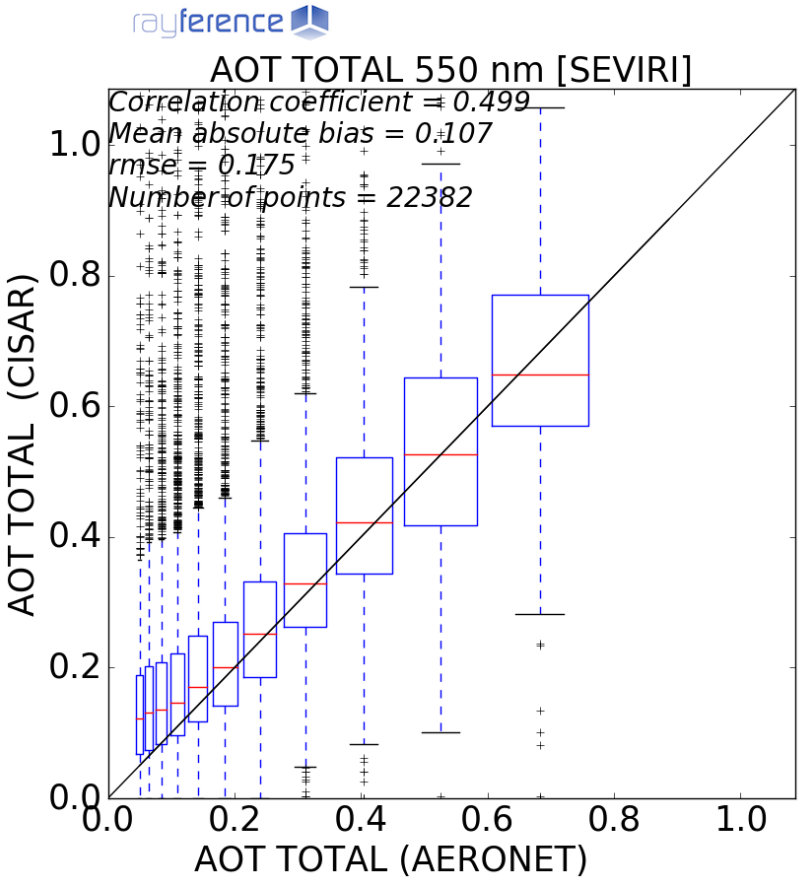


- All figures should be re-plotted with fonts at least twice in size

Figure fonts have been enlarged.

- I trust that in Figure 2 now the arrows have lengths proportional to the discussed changes. Nonetheless, more wavelengths would be needed to make the figure informative. Perhaps, it could be made into a two-panel figure with Fig. 3?

Wavelengths 0.55 to 0.87 have a behaviour very close to 0.44. Hence, adding these wavelengths to Figure 2 provides pretty confusing results.

- Figures 6-12 should be merged in a single figure (or two).

These Figures are split to avoid having an endless single Figure that can be far away from the text. Splitting the Figures allows to keep the Figures close to the text.

- The comments to Figs. 6 and 7 confuse me: for example, in Fig. 6 it is said that w_0 is well retrieved and the g parameter systematically underestimated, but the figure shows the opposite. Similar arguments hold for Fig. 7 (g no longer systematically underestimated, w_0 slightly underestimated).

In Figure 6, the truth w_0 values lay between 0.94 and 0.95 while the retrieved ones between 0.91 and 0.95. This parameter is therefore quite well retrieved as stated in the text. Considering the asymmetry parameter g, the truth values in band 0.87 is 0.58 and the retrieved one 0.48. This underestimation in the retrieved values is also present for the other bands.

- Could you make Table 6 into a figure instead? The would also eliminate the need for Table 5, since the true values could be pitted as you did for Figs. 7-12.

We think that in case of the RPV parameters a table is sufficient to fully understand the performances of CISAR and we do not want to add even more and unnecessary figures to the paper.

L23: This is not universally true. what about absorbing aerosols? what about very large optical depths? Could you prove that enhanced forward scattering does NOT highlight anisotropy? Such claims at least call for appropriate references

An in-depth understanding of the radiative coupling effects between diffuse sky radiation and surface reflectance anisotropy. For instance, when the scattering optical thickness becomes very large, surface behaves almost as a Lambertian one as no shadows are present anymore. This is pretty independent from the type of aerosols. This is what it is stated in our sentence. We also say, "In most cases" and not "Always". This statement would be erroneous for a shadowless type of surface, which does not exist on Earth. References where the effects of this coupling are illustrated have been added to the text.

L52 what's the difference between these two aspects?

These sentences read now:

Firstly, only a limited region of the solution space is sampled as a result of the reduced range of variability for state variables. For instance, in order to reduce the size of the LUTS, Pinty et al. (2000b) limit the maximum aerosol optical thickness to 1. Secondly, the solution space is not continuously sampled due to the use of pre-defined aerosol classes.

L94 could you add a sentence of whether this issue is still of concern? What did Luffarelli et al 2016 concluded?

The sentence reads now:

This latter issue has been addressed by Luffarelli et al. (2016) who retrieve an aerosol optical thickness value for each SEVIRI observation.

L130 The connection between Dubovik's classes and the ones in Fig. 1 must be made clear. All I get from the figures is the strange impression that the fine mode is spherical and the coarse mode is non-spherical.

That is indeed the case

Manuscript prepared for Atmos. Meas. Tech.
with version 4.2 of the LaTeX class copernicus.cls.
Date: 12 June 2017

# Joint retrieval of surface reflectance and aerosol properties with continuous ~~variations~~ variation of the state variables in the solution space: Part 1: theoretical concept

Yves Govaerts[1] and Marta Luffarelli[1]

[1]Rayference, Brussels, Belgium

*Correspondence to:* Yves Govaerts (yves.govaerts@rayference.eu)

**Abstract.** This paper presents a new algorithm for the joint retrieval of surface reflectance and aerosol properties with continuous variations of the state variables in the solution space. This algorithm, named CISAR (Combined Inversion of Surface and AeRosol), relies on a simple atmospheric vertical structure composed of two layers and an underlying surface. Surface anisotropic reflectance effects are taken into account and radiatively coupled with atmospheric scattering. For this purpose, a fast radiative transfer model has been explicitly developed, which includes acceleration techniques to solve the radiative transfer equation and to calculate the Jacobians. The inversion is performed within an optimal estimation framework including prior information on the state variable magnitude and regularization constraints on their spectral and temporal variability. In each processed wavelength, the algorithm retrieves the parameters of the surface reflectance model, the aerosol total column optical thickness and single scattering properties. The CISAR algorithm functioning is illustrated with a series of simple experiments.

## 1 Introduction

Radiative coupling between atmospheric scattering and surface reflectance processes prevents the use of linear relationships for the retrieval of aerosol properties over land surfaces. The discrimination between the contribution of the signal reflected by the surface and that scattered by aerosols represents one of the major issues when retrieving aerosol properties using spaceborne imager observations over land surfaces. Conceptually, this problem is equivalent to solving a radiative system composed of at least two layers, where the upper layers include aerosols and the bottom ~~one(s) represent (s)~~ ones represent the soil/vegetation strata. The problem is further complicated by the

intrinsic anisotropic radiative behaviour of natural surfaces due to the mutual shadowing of the scattering elements, which is also affected by the amount of sky radiation (Govaerts et al., 2010, 2016). In most ~~of the case~~cases, an increase in aerosol concentration is responsible for an increase ~~of~~ in the fraction of diffuse sky radiation which, in turn, smooths the effects of surface reflectance anisotropy. Though multi-spectral information is critical for the retrieval of aerosol properties, the spectral dimension alone does not allow ~~to fully characterise~~ full characterisation of the underlying surface reflectance which often offers a significant contribution to the total signal observed at the satellite level. ~~Hence, the exploitation of~~ In this regard, the additional information contained in multi-spectral and multi-angular observations through the joint retrieval of surface reflectance and aerosol properties has proven to be an efficient way to characterize aerosol properties over land surfaces.

Pinty et al. (2000a) pioneered the development of a retrieval method dedicated to the joint retrieval of surface reflectance and aerosol properties based on the inversion of a physically-based radiative model. This method has been subsequently improved to allow the processing of any geostationary satellites accounting for their actual radiometric performance (Govaerts and Lattanzio, 2007). This new versatile version of Pinty's algorithm has permitted the generation of a global surface albedo product ~~generated~~ from archived data acquired by operational geostationary satellites around the globe (Govaerts et al., 2008). These data included observations acquired by an old generation of radiometers with only one broad solar channel on-board the European Meteosat First Generation satellite, the US Geosynchronous Operational Environmental Satellite (GOES) and the Japanese Geostationary Meteorological Satellite (GMS). It is now routinely applied in the framework of the Sustained and COordinated Processing of Environmental satellite data for Climate Monitoring (SCOPE-CM) initiative for the generation of essential climate variables (Lattanzio et al., 2013). An improved version of this algorithm has been proposed by Govaerts et al. (2010) to take advantage of the multi-spectral capabilities of Meteosat Second Generation Spinning Enhanced Visible and Infrared Imager (MSG/SEVIRI) operated by EUMETSAT, and includes an Optimal Estimation (OE) inversion scheme using a minimization approach based on the Marquardt-Levenberg method (Marquardt, 1963).

The strengths and weaknesses of the algorithm proposed by Govaerts et al. (2010) are discussed in Section (2). In their proposed approach, the solutions of the Radiative Transfer Equation (RTE) are pre-calculated and stored in Look-Up Tables (LUTs) for a limited number of state variable values. Aerosol properties are limited to six different classes dominated either by fine or coarse particles. ~~In an OE context, two~~ Two major drawbacks result from the use of pre-defined aerosol classes stored in pre-computed LUTs. Firstly, only a limited region of the solution space is sampled as a result of the reduced range of variability for state variables. For instance, in order to reduce the size of the LUTS, Pinty et al. (2000b) limit the maximum aerosol optical thickness to 1. Secondly, the solution space is not continuously sampled due to the use of pre-defined aerosol classes. Such an approach prevents an accurate retrieval of the solution at the expense of a very large number of classes. Dubovik et al.

(2011) and Diner et al. (2012)~~among others~~ , among others, demonstrated the advantages of a retrieval approach based on continuous variations of the aerosol properties as opposed to a LUT-based approach relying on a set of pre-defined aerosol classes. Even ~~when~~ considering a large number of aerosol classes, LUT-based approaches under-perform methods with multi-variate continuity in the solution space (Kokhanovsky et al., 2010).

A new joint surface reflectance / aerosol properties retrieval approach is presented here that overcomes the limitations resulting from pre-computed RTE solutions stored in LUTs. This new method takes advantage of the lessons learned from past attempts to retrieve simultaneously surface reflectance and aerosol properties. The advantages of a continuous variation of the aerosol properties in the solution space against a LUT-based approach is discussed in Section (3). The proposed method expresses the scattering albedo and phase function values as a linear mixture of basic aerosol classes. The forward radiative transfer model that includes the Jacobians computation is described in Section (4). With the exception of gaseous transmittance, this model no longer relies on LUTs, and the RTE is explicitly solved. The inversion method is described in Section (5). Finally, the ~~behaviour of this algorithm~~ possibility to express aerosol single scattering properties as a linear combination is illustrated with simulated data representing various scenarios including small and large particles (6).

## 2 Lessons learned from previous approaches

Pinty et al. (2000a) proposed an algorithm for the joint retrieval of surface reflectance and aerosol properties to demonstrate the possibility of generating Essential Climate Variables (ECV) from data acquired by operational weather geostationary satellites. Due to limited operational computational resources available at that time in the EUMETSAT ground segment, where the data were processed, the development of this algorithm was subject to strong constraints. The RTE solutions were pre-computed and stored in LUTs with a very coarse resolution, limiting the maximum Aerosol Optical Thickness (AOT) to ~~1. It represents a sever~~ 1, which represented a severe limitation over the Sahara region where AOT values can easily exceed such limit. Furthermore, the radiative coupling between aerosol scattering and gaseous absorption was not taken into account. This algorithm, referred to as Geostationary Surface Albedo (GSA) has been subsequently modified by Govaerts and Lattanzio (2007) to include an estimation of the retrieval uncertainty. This updated version has permitted the generation of a global aerosol product derived from observations acquired by operational weather geostationary satellites (Govaerts et al., 2008). Since then, it is routinely applied in the framework of the SCOPE-CM initiative ~~for~~ to generate a Climate Data Record (CDR) ~~generation~~ of surface albedo (Lattanzio et al., 2013).

The GSA algorithm has been further improved for the processing of SEVIRI data on-board MSG for the retrieval of the total column AOT from observations acquired in the VIS0.6, VIS0.8 and NIR1.6 spectral bands (Govaerts et al., 2010; Wagner et al., 2010). The method developed by these

authors relies on an OE approach where surface reflectance and daily aerosol load are simultaneously retrieved. The inversion is performed independently for each aerosol class and the one with the best fit is selected. A physically-based radiative transfer model accounting for non-Lambertian surface reflectance and its radiative coupling with ~~the~~ atmospheric scattering is inverted against daily accumulated SEVIRI observations. However, this Land Daily Aerosol (LDA) algorithm suffers from two major limitations: (*i*) the use of pre-defined aerosol classes and, (*ii*) the algorithm delivers only one mean aerosol value per day when applied on MSG/SEVIRI data. This latter issue has been addressed ~~elsewhere (Luffarelli et al., 2016)~~by Luffarelli et al. (2016) who retrieve an aerosol optical thickness value for each SEVIRI observation. The former issue prevents a continuous variations of the state variables characterizing the aerosol single scattering properties as required by an OE approach (Rodgers, 2000). ~~Consequently, a~~ A consistent implementation of such approach is not straightforward since aerosol classes are defined as ~~a~~ prior knowledge of the observed medium but no uncertainties are assigned to this information~~preventing the estimation of the corresponding retrieval uncertainty~~. Consequently, the estimated retrieval retrieval uncertainty is inconsistent as it does not account for the use of prior information and associated uncertainties.

Diner et al. (2012) demonstrated the advantages of a retrieval method based on continuous variations of aerosol single scattering properties in the solution space as opposed to a LUT-based approach derived for a limited number of pre-defined aerosol classes. Dubovik et al. (2011) proposed an original method for the retrieval of aerosol micro-physical properties which also does not necessitate the use of predefined aerosol classes. This method retrieved more than 100 state variables requiring therefore a considerable ~~amount~~ number of observations, such as those provided by multi-angular and -polarisation ~~radiometer~~ radiometers like Polarisation et Anisotropie des Réflectances ~~au~~ Au SOmmet de l'Atmosphère (PARASOL) (Serene and Corcoral, 2006) or the future Multi-viewing Multi-channel Multi-polarization Imaging (3MI) instrument on-board EUMETSAT's Polar System Second Generation (Manolis et al., 2013). Instruments delivering such a large ~~amount~~ number of observations are rather scarce as most of the current or planned passive optical sensors do not offer instantaneous multi-angular observation capabilities nor information on polarization. The primary objective of this paper is to address the limitations resulting from conventional approaches based on LUTs and/or a limited number of pre-defined aerosol classes, proposing a method that can be ~~easily applied on~~ applied to observations acquired by single or multi-view ~~imager~~ instruments.

## 3 Continuous variation of aerosol properties in the solution space

Aerosol single scattering properties include the single scattering albedo $\omega_0$ and the phase function $\Phi$ in RTE. Govaerts et al. (2010) explained the benefits of representing pre-defined aerosol classes in a two-dimensional solution space composed of these aerosol single scattering properties. For the sake of clarity, they limited the phase function in that 2D space to the first term of the Legendre

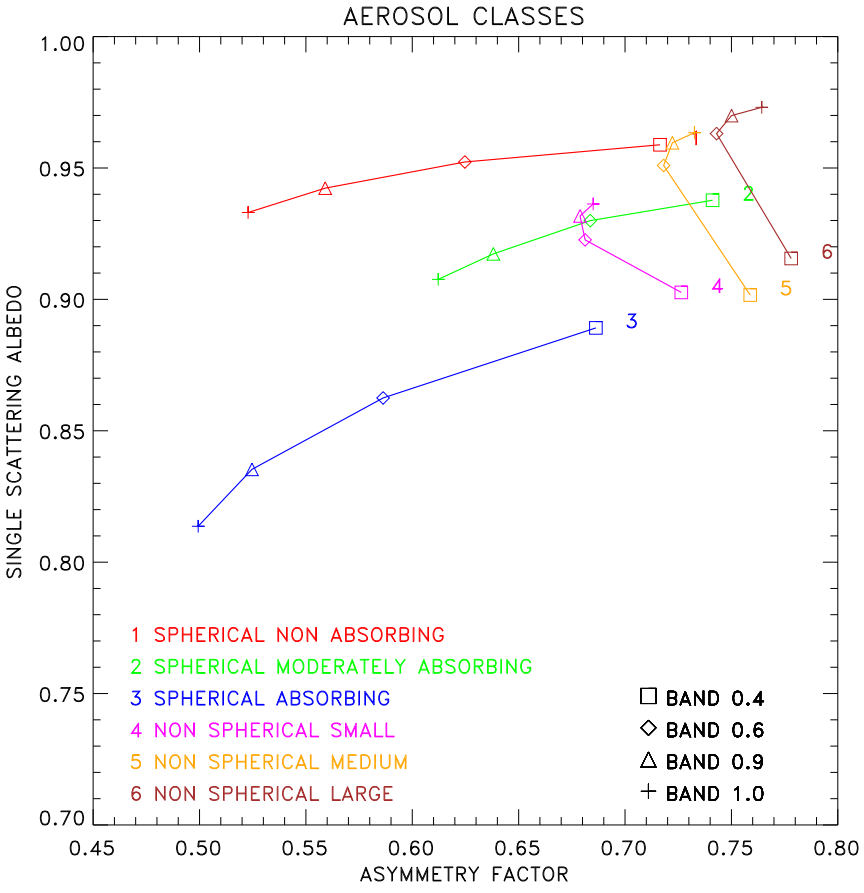


**Fig. 1.** Aerosol dual mode classes after Govaerts et al. (2010) in the $[g,\omega_0]$ space derived from the aggregation of aerosol single scattering properties retrieved from AERONET observations (Dubovik et al., 2006). Classes 1 to 3 are dominated by the fine mode and 4 to 6 by the coarse one.

coefficients, *i.e.*, the asymmetry parameter $g$. However, one should keep in mind that the reasoning applied in this Section should ~~actually~~ be applied on the entire phase function $\Phi$~~only~~. These aerosol single scattering properties are themselves determined by aerosol micro-physical properties such as the particle size distribution, shape and their complex index of refraction. Within a retrieval approach based on aerosol classes, the objective is to provide the best possible sampling of the $[g,\omega_0]$ space such as in Govaerts et al. (2010). The inversion process proposed by these authors relies on a set of six classes which have been defined from AErosol RObotic NETwork (AERONET) data aggregation (Dubovik et al., 2006). These classes are supposed to provide the most likely sampling of the solution space but, since the scattering properties are not continuously varied, the inversion is typically repeated for each aerosol class and the one with the best fit is selected (Wagner et al., 2010).

A visual inspection of Fig. (1) after Govaerts et al. (2010) reveals that aerosol classes occupy

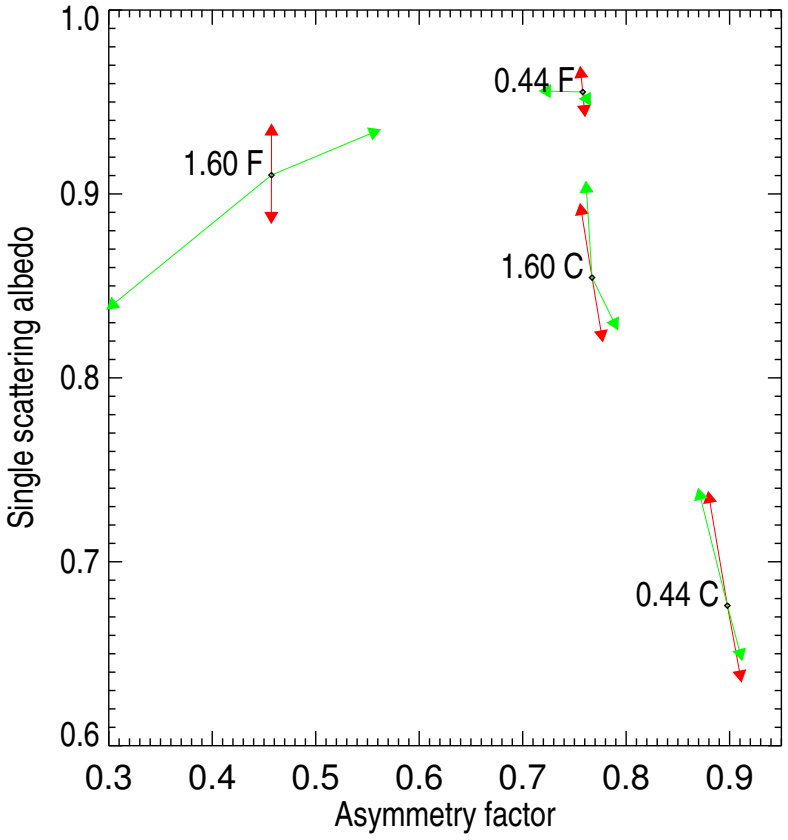


**Fig. 2.** Example of sensitivity of aerosol single scattering properties to particle median radius (green arrows) and imaginary part of the refractive index (red arrows) at 0.44$\mu$m and 1.60$\mu$m for fine mode F ($r_{mf} = 0.1\mu m$) and coarse mode C ($r_{mc} = 2.0\mu m$).

different regions in the $[g,\omega_0]$ space according to the dominant particle size distribution, *i.e.*, fine or coarse. Within that space, an aerosol class is defined by the spectral behaviour of $\{g(\lambda),\omega_0(\lambda)\}$ pairs. The proposed fine mode classes vary ~~essentially~~ mostly as a function $\omega_0$ which is largely determined by the imaginary part of the refractive index $n_i$. Conversely, aerosol classes dominated by coarse particles show little dependency on $g$ and are therefore organised parallel to the single scattering albedo axis. The main parameter discriminating these latter classes is the median radius $r_m$, which essentially determines the asymmetry parameter value at a given wavelength $\lambda$.

To illustrate the dependence of $g$ and $\omega_0$ on the median radius $r_m$ and imaginary part of the refractive index $n_i$, fine and coarse mono-mode aerosol classes have been generated with $r_m = 0.15\mu m$ and 2.0$\mu$m respectively. The other micro-physical values have been fixed to $\sigma_r = 0.5\mu m$ $n_r = 1.42$ and $n_i = 0.008$ where $\sigma_r$ is the radius standard deviation and $n_r$ the real part of the refractive index. These values have been selected on purpose to ~~explain the~~ ease the explanation of

the aerosol classes organisation on Fig. (1). Black dots on Fig. (2) show the corresponding location of the pair of $\{g(\lambda),\omega_0(\lambda)\}$ values at 0.44$\mu$m and 1.60$\mu$m. Red arrows illustrate the sensitivity to a $n_i$ change of $\pm 0.0025$ and the green ones to a $r_m$ change of $\pm 25\%$. For the fine mono-mode (F), changes in $n_i$ essentially translate in displacement parallel to the $\omega_0$ axis at short wavelengths while changes in $r_m$ result in changes parallel to the $g$ axis. There is also a clear relationship between the particle size and $g$ for that mode. A change in the particle size results in a change in $g$ while $\omega_0$ remains almost unchanged. The situation is quite different for the coarse mono-mode where changes in both $n_i$ and $r_m$ induce displacement parallel to the $\omega_0$ axis with limited impact on $g$ values. It should also be noted that the direction and magnitude of the changes depend on the wavelengths.

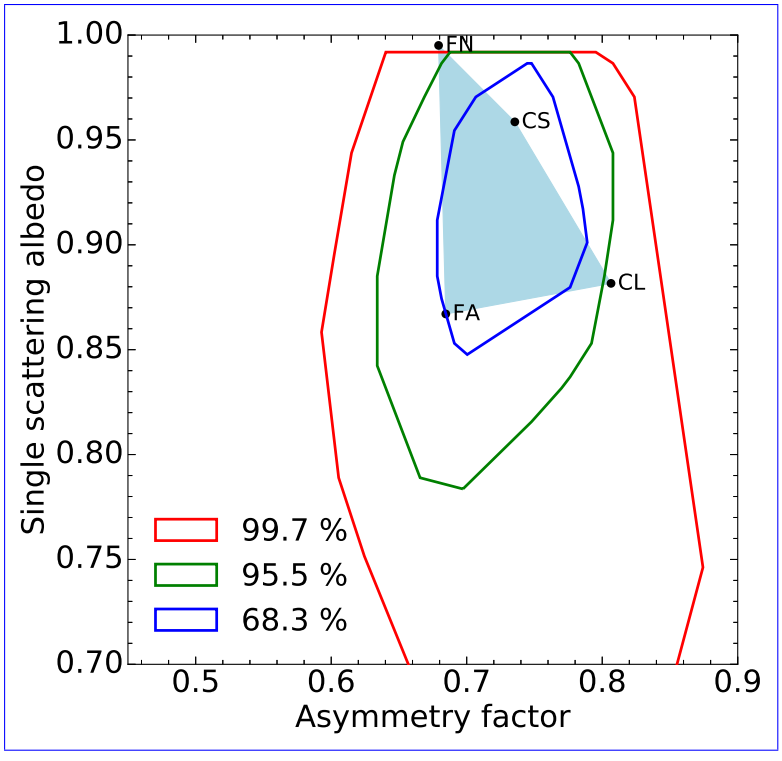


**Fig. 3.** Example of region (~~red~~ light blue area) in the $[g,\omega_0]$ solution space at ~~0.55~~0.44$\mu$m defined by four aerosol vertices: single fine mode non-absorbing (FN), single fine mode absorbing (FA), coarse mode with small radius (CS) and coarse mode with large radius (CL). The isolines show the probability that the aerosol single scattering properties derived from Dubovik et al. (2006) fall within the delineated spaces.

The actual extent of possible solutions in the $[g,\omega_0]$ space for a given spectral band can be outlined by a series of vertices characterizing aerosol single scattering properties. Following Fig. (2), these vertices are defined by an absorbing and a non-absorbing fine mono-mode classes with a small radius, labelled respectively FA and FN and by two coarse mono-modes with different radii, *i.e.*, large and small, labelled respectively CL and CS. Such vertices define a polygon within the $[g,\omega_0]$ solution space (Fig. ??3). The number of vertices can be adjusted according to the amount of

spectral observations and expected type of aerosols. In Section (4), we will see how any pair of single scattering albedo and phase function values in that space can be expressed as a linear ~~mixture of the vertices properties.~~ combination of the vertex properties.

The choice of the position of these vertices is critical as they should encompass most likely aerosol single scattering properties that could be observed at a given time and location. Different approaches could be used to define the position of these vertices. These positions could be derived from the analysis of typical aerosol single scattering properties available in databases such as Optical Properties of Aerosols and Clouds (OPAC) (Hess et al., 1998). Alternatively, it is also possible to follow a similar approach as the one proposed in Govaerts et al. (2010) who analysed the single scattering albedo and phase function values derived from AERONET observations acquired in a specific region of interest for a given period (Dubovik et al., 2006). Fig. (3) shows an example of such type of analysis performed in the blue spectral region. The red isoline on that Fig. delineates the area of the $[g,\omega_0]$ space where 99.7% of the aerosol single scattering properties derived by Dubovik et al. (2006) from AERONET observations are located. The green and blue lines show respectively the 95% and 68% probability regions. These values have been derived using all available Level 2 AERONET observations since 1993. Finally, the model proposed by Schuster et al. (2005) can be used to determine the spectral variations of the single scattering properties outside the spectral bands measured by AERONET. The present study relies on simulated data and the aerosol vertices have been positioned to sample the solution space in a realistic way. In case of the processing of actual satellite data over a specific region or period, it is advised to calculate the isolines corresponding to that region of interest from AERONET observations and to adjust the position of the aerosol vertices accordingly.

## 4 Forward Radiative Transfer Model

### 4.1 Overview

The forward model, named FASTRE, simulates the TOA Bidirectional Reflectance Factor (BRF) $y_m(\mathbf{x},\mathbf{b};\mathbf{m})$ as a function of ~~the viewing and illumination angles, the wavelength and~~ independent parameters $\mathbf{m}$ defining the observation conditions and a series of state variables $\mathbf{x}$ describing the state of the atmosphere and underlying surface. ~~The TOA reflectance depends on the retrieved state variables $\mathbf{x}$, the model parameters $\mathbf{b}$ and finally the observation conditions. Model parameters represent variables~~ Model parameters $\mathbf{b}$ represent variables such as total column water vapour that influence the value of $y_m(\mathbf{x},\mathbf{b};\mathbf{m})$ but cannot be retrieved from the processed space-based observations due to the lack of independent information. The independent parameters ~~, such as~~ $\mathbf{m}$ include the illumination and viewing geometries $(\Omega_0,\Omega_v)$ ~~or~~ and the spectral bands $\tilde{\lambda}$~~, characterize the observation conditions and are denoted $\mathbf{m}$~~. The RTE is solved with the Matrix Operator Method (Fischer and Grassl, 1984) optimised by Liu and Ruprecht (1996) for a limited number of quadrature points.

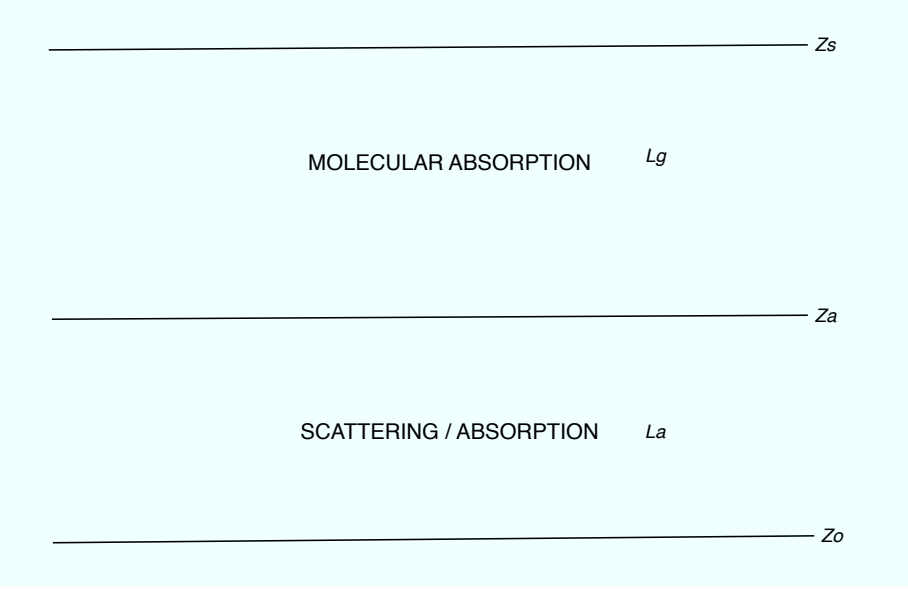


**Fig. 4.** Vertical structure of the FASTRE model. The surface is at level $Z_0$ and radiatively ~~couple~~ coupled with the lower layer $L_a$ running from level $Z_0$ to $Z_a$. This layer includes scattering and absorption processes. The upper layer $L_g$ runs from level $Z_a$ to $Z_s$ and only accounts for absorption processes.

The model simulates observations acquired within spectral bands $\tilde{\lambda}$ characterized by their spectral response. Gaseous transmittances in these bands are precomputed and stored in LUTs. All other operations are calculated on the fly. The model computes ~~separately~~ the contributions from single and multiple scattering separately, the latter being solved in Fourier space. In order to reduce the computation time, the forward model relies on the same atmospheric vertical structure as in Govaerts et al. (2010), *i.e.*, a three-level system containing two layers that are radiatively coupled (Fig. 4). The lowest level, $Z_0$, represents the surface. The lower layer $L_a$, ranging from levels $Z_0$ to $Z_a$ ~~hosts the aerosols~~, contains the aerosol particles. Molecular scattering and absorption are also taking place in that layer which is radiatively coupled with the surface for both the single and the multiple scattering. The upper layer $L_g$, ranging from $Z_a$ to $Z_s$, is only subject to molecular absorption. It is assumed that no scattering processes are taking place in that layer.

The surface reflectance $r_s(\mathbf{x_s},\mathbf{b};\mathbf{m})$ over land is represented by the so-called RPV (Rahman-Pinty-Verstraete) model which has four parameters $\mathbf{x_s} = \{\rho_0, k, \Theta, h\}$ that are all wavelength dependent (Rahman et al., 1993). Each of these parameters control surface BRF differently. The $\rho_0$ parameter, included in the [0,1] interval, controls the mean amplitude of the BRF and strongly varies with wavelengths. The $k$ parameter is the modified Minnaert's contribution that determines the bowl or bell shape of the BRF and it typically varies between 0 and 2. The asymmetry parameter of the Henyey-Greenstein phase function, $\Theta$, varies between -1 and 1. The $h$ parameter controls the amplitude of the hot-spot due to the "porosity" of the medium. This parameter takes only positive values

and generally varies between 0 and 1. For the simulations over the ocean, the Cox-Munk model (Cox and Munk, 1954) is implemented (Vermote et al., 1997).

Aerosol single scattering properties in the layer $L_a$ are represented by an external mixture of a series of predefined aerosol vertices as explained in Section (4.2). The $L_g$ layer contains only absorbing gas not included in the scattering layer, such as high-altitude ozone, the part of the total column water vapour not included in layer $L_a$ and few well-mixed gases.

~~FASTRE~~ The FASTRE model expresses the TOA BRF in a given spectral band $\tilde{\lambda}$ as a sum of the single $I_s^{\uparrow}$ and multiple $I_m^{\uparrow}$ scattering contributions ~~with~~ as in

$$y_m(\mathbf{x},\mathbf{b};\mathbf{m}) = T_{L_g}(\mathbf{b};\mathbf{m})\,\frac{I_s^{\uparrow}(\mathbf{x},\mathbf{b};\mathbf{m}) + I_m^{\uparrow}(\mathbf{x},\mathbf{b};\mathbf{m})}{E_0^{\downarrow}(\mathbf{m})\mu_0} \tag{1}$$

where

. $I_s^{\uparrow}(\mathbf{x},\mathbf{b};\mathbf{m})$ is the upward radiance field at level $Z_a$ due to the single scattering;

. $I_m^{\uparrow}(\mathbf{x},\mathbf{b};\mathbf{m})$ is the upward radiance field at level $Z_a$ due to the multiple scattering;

. $T_{L_g}(\mathbf{b};\mathbf{m})$ denotes the total transmission factor in the $L_g$ layer;

. $E_0^{\downarrow}(\mathbf{m})$ denotes the solar irradiance at level $Z_s$ corrected for the Sun-Earth distance variations.

The single scattering contribution writes

$$I_s^{\uparrow}(\mathbf{x},\mathbf{b};\mathbf{m}) = \frac{E_0^{\downarrow}(\mathbf{m})\,\mu_0}{\pi}\exp\left(\frac{-\tau_{L_a}}{\mu_0}\right) r_s(\mathbf{x_s},\mathbf{b};\mathbf{m})\exp\left(\frac{-\tau_{L_a}}{\mu_v}\right) \tag{2}$$

where $\tau_{L_a}$ is the total optical thickness of layer $L_a$. $\mu_0$ and $\mu_v$ are the cosine of the illumination and viewing zenith angles respectively.

The multiple scattering contribution $I_m^{\uparrow}(\mathbf{x},\mathbf{b};\mathbf{m})$ is solved in the Fourier space in all illumination and viewing directions of the quadrature directions $N_\theta$ for $2N_\theta - 1$ azimuthal directions. The contribution $I_m^{\uparrow}(\mathbf{x},\mathbf{b};\mathbf{m})$ in the direction $(\Omega_0,\Omega_v)$ is interpolated from the surrounding quadrature directions. Finally, the ~~Jacobians $\mathbf{k}_x = \frac{\partial y_m(\mathbf{x},\mathbf{b};\mathbf{m})}{\partial x}$~~ Jacobian $\mathbf{k}_{x_i} = \frac{\partial y_m(\mathbf{x_i},\mathbf{b};\mathbf{m})}{\partial x_i}$ of $y_m(\mathbf{x},\mathbf{b};\mathbf{m})$ for parameter $x_i$ are calculated as finite differences.

### 4.2 Scattering layer $L_a$ properties

The layer $L_a$ contains a set of mono-mode aerosol classes $v$ characterized by their single scattering properties, *i.e.*, the single scattering albedo $\omega_{0,v}(\tilde{\lambda})$ and phase function ~~$\Phi_v(\tilde{\lambda})$~~ $\Phi_v(\tilde{\lambda},\Omega_g)$ in the spectral bands $\tilde{\lambda}$ at the phase angle $\Omega_g$. These classes define the vertices encompassing the solution space, as illustrated in Fig. (~~??~~). ~~These~~ 3). The different vertices representing fine and coarse mode aerosols are combined into this layer according to their respective optical thickness $\tau_v(\tilde{\lambda})$ with the total aerosol optical thickness $\tau_a(\tilde{\lambda})$ of the layer being equal to

$$\tau_a(\tilde{\lambda}) = \sum_v \tau_v(\tilde{\lambda}) \tag{3}$$

~~Each phase function $\Phi_v(\tilde{\lambda})$ of the various aerosol vertices~~ The phase function $\Phi_v(\tilde{\lambda},\Omega_g)$ of an aerosol vertex is characterized by a limited number $N_\kappa$ of Legendre coefficients equal to $2N_\theta - 1$ where $N_\theta$ is the number of quadrature points used to solve the multiple scattering integral. The choice of this number results from a trade-off between accuracy and computer time. When $N_\kappa$ is too small, the last Legendre moment is often not equal to zero and the delta-M approximation is applied (Wiscombe, 1977). In that case, the $\alpha_d$ coefficient of the delta-M approximation is equal to $\Phi_v(N_\kappa)$. The Legendre coefficients $\kappa_j$, after application of the delta-M approximation, become

$$c_j = \frac{\kappa_j - \alpha_d}{1 - \alpha_d} \tag{4}$$

and the truncated phase function denoted $\Phi'_v$. The corrected optical thickness $\tau'_v(\tilde{\lambda})$ and single scattering albedo $\omega'_{0,v}(\tilde{\lambda})$ of the corresponding aerosol class become

$$\tau'_v(\tilde{\lambda}) = (1 - \omega_{0,v}\alpha_d)\tau_v(\tilde{\lambda}) \tag{5}$$

and

$$\omega'_{0,v}(\tilde{\lambda}) = \frac{1 - \alpha_d}{1 - \omega_{0,v}\alpha_d}\omega_{0,v}(\tilde{\lambda})\,. \tag{6}$$

The layer total optical thickness, $\tau_{L_a}$, is the sum of the gaseous, $\tau_g$, the aerosol, ~~$\tau_a$~~ $\tau'_a$ and the Rayleigh, $\tau_r$, optical depth

$$\tau_{L_a}(\tilde{\lambda}) = \tau_g(\tilde{\lambda}) + \sum_v \tau_a{}'_v(\tilde{\lambda}) + \tau_r(\tilde{\lambda}) \tag{7}$$

with $\tau'_a(\tilde{\lambda}) = \sum_v \tau'_v(\tilde{\lambda})$. The single scattering albedo of the scattering layer is equal to

$$\omega'_0(\tilde{\lambda}) = \frac{\sum_c \omega'_{0,v}(\tilde{\lambda})\,\tau'_v(\tilde{\lambda})}{\tau_a(\tilde{\lambda})} \frac{\sum_c \omega'_{0,v}(\tilde{\lambda})\,\tau'_v(\tilde{\lambda})}{\tau'_a(\tilde{\lambda})} \tag{8}$$

and the layer average phase function

$$\Phi'(\tilde{\lambda},\Omega_g) = \frac{\sum_c \Phi'_v(\tilde{\lambda})\,\tau'_v(\tilde{\lambda})}{\tau_a(\tilde{\lambda})} \frac{\sum_c \Phi'_v(\tilde{\lambda},\Omega_g)\,\tau'_v(\tilde{\lambda})}{\tau'_a(\tilde{\lambda})}\,. \tag{9}$$

### 4.3 Gaseous layer properties

It is assumed that only molecular absorption is taking place in layer $L_g$. The height of level $Z_a$ is used to partition the total column water vapour and ozone concentration in each layer assuming a US76 standard atmosphere vertical profile. This height is not retrieved and is therefore a model parameter of FASTRE which should be derived from some climatological values. $T_{L_g}$ denotes the total transmission of that layer.

**Table 1.** Relative bias and root mean square error in percentage between FASTRE and the reference RTM in various spectral bands. Wavelengths are given in $\mu$m.

| Spectral bands ($\mu$m) | 0.44 | 0.55 | 0.67 | 0.87 |
|---|---|---|---|---|
| Relative bias (%) | ~~-1.09~~ -1.1 | ~~-0.32~~ -0.3 | ~~0.00~~ 0.0 | ~~+0.32~~ 0.3 |
| Relative RMSE (%) | ~~2.78~~ 2.8 | ~~1.79~~ 1.8 | ~~1.30~~ 1.3 | ~~1.23~~ 1.2 |

### 4.4 FASTRE model accuracy

The simple atmospheric vertical structure composed of two layers is the most important assumption of the FASTRE model. In order to evaluate the accuracy of FASTRE, a similar procedure as in Govaerts et al. (2010) has been applied. The outcome of FASTRE has been evaluated against a more elaborated 1D Radiative Transfer Model (RTM) (Govaerts, 2006) where the vertical structure of the atmosphere is explicitly taken into account for sun and viewing angles varying from 0 to 70°, for various types of aerosols, surface reflectance and total column water vapour values. The mean relative bias and relative Root Mean Square Error (RMSE) between the reference model and FASTRE have been estimated in the main spectral bands used for aerosol retrieval. The relative RMSE, $R_r$, is estimated with

$$R_r = \sqrt{\frac{1}{N}\sum_{N}\left(\frac{y_m(\mathbf{x},\mathbf{b};\mathbf{m}) - y_r(\mathbf{x},\mathbf{b};\mathbf{r})}{y_r(\mathbf{x},\mathbf{b};\mathbf{r})}\right)^2} \tag{10}$$

where $y_r(\mathbf{x},\mathbf{b};\mathbf{m})$ is the TOA BRF calculated with the reference model. In this paper, the FASTRE model solves the RTE using 16 quadrature points $N_\theta$ which provides a good compromise between speed and accuracy. Results are shown on Table (1). As can be seen, ~~in most of the bands the~~ the relative RMSE between FASTRE and the reference model is typically in the range of 1% – ~~2%. Slightly larger values are observed at longer wavelengths due to a higher sensitivity to the atmospheric vertical structure in these spectral regions~~3%. A similar comparison has been performed against actual PROBA-V observations (Luffarelli et al., 2017). These comparisons show a root mean square error between simulated and actual observations in the range 0.024–0.038.

## 5 Inversion process

### 5.1 Overview

Surface reflectance characterisation requires multi-angular observations $\mathbf{y}_{\Omega\tilde{\Lambda}}$, the acquisition of which can take between several minutes, as is the case for the Multi-angle Imaging SpectroRadiometer (MISR) instrument, and several days, as is the case for the Ocean and Land Colour Instrument (OLCI) on-board Sentinel-3 or the Moderate Resolution Imaging Spectroradiometer (MODIS). In

the former case, data are often assumed being acquired almost instantaneously, *i.e.*, ~~a situation where most likely~~ with the atmospheric properties ~~remain~~ remaining unchanged during the acquisition time. Such situation considerably reduces the calculation time required to solve the RTE, as the multiple scattering term $I_m^{\uparrow}(\mathbf{x},\mathbf{b};\mathbf{m})$ needs to be estimated only once per spectral band. In the latter case, atmospheric properties cannot be assumed to be invariant and the multiple scattering contribution needs to be solved for each observation. When geostationary observations are processed, the accumulation period is often reduced to one day, and the assumption that the atmosphere does not change can be converted into an equivalent radiometric uncertainty (Govaerts et al., 2010). Strictly speaking, it should be ~~necessary to assume~~ assumed that atmospheric properties have changed when the accumulation time ~~exceed several minutes as in Luffarelli et al. (2016), which increase~~ exceeds several minutes (Luffarelli et al., 2016), which increases the number of retrieved state variables to taken into account and therefore the processing time.

The retrieved state variables in each spectral band $\widetilde{\lambda}$ are composed of the $\mathbf{x_s}$ parameters characterising the state of the surface and the set of aerosol optical thicknesses $\tau_v$ ~~of the respective~~ for the aerosol vertices that are mixed in layer $L_a$. Prior information consists of the expected values $\mathbf{x_b}$ of the state variables ~~characterising the state of the~~ $\mathbf{x}$ characterising the surface and the atmosphere on one side~~and regularization on~~ , and regularization of the spectral and/or temporal variability of $\tau_v$ on the other side. Uncertainty matrices $\mathbf{S}_x$ are assigned to this prior information. Finally, uncertainties in the measurements $\mathbf{S}_y$ are assumed to be normally distributed with zero mean. The inversion process of the FASTRE model will be ~~further~~ herein referred to as Combined Inversion of Surface and AeRosol (CISAR) algorithm.

### 5.2 Cost function

The fundamental principle of Optimal Estimation (OE) is to maximise the probability $P = P(\mathbf{x}|\mathbf{y}_{\Omega\widetilde{\Lambda}},\mathbf{x_b},\mathbf{b})$ with respect to the values of the state vector $\mathbf{x}$, conditional to the value of the measurements and any prior information. The conditional probability takes on the quadratic form ~~(Rodgers, 2000)~~(Rodgers, 2000; Dubovik et al., 2011):

$$
\begin{aligned}
P(\mathbf{x}) \propto \exp & \left[ -\left(y_m(\mathbf{x},\mathbf{b};\mathbf{m}) - \mathbf{y}_{\Omega\tilde{\Lambda}}\right)^T \mathbf{S}_y^{-1} \left(y_m(\mathbf{x},\mathbf{b};\mathbf{m}) - \mathbf{y}_{\Omega\tilde{\Lambda}}\right) \right] \\
& \exp \left[ -\left(\mathbf{x} - \mathbf{x}_b\right)^T \mathbf{S}_x^{-1} \left(\mathbf{x} - \mathbf{x}_b\right) \right] \\
& \exp \left[ -\mathbf{x}^T \mathbf{H}_a^T \mathbf{S}_a^{-1} \mathbf{H}_a \mathbf{x} \right] \\
& \exp \left[ -\mathbf{x}^T \mathbf{H}_l^T \mathbf{S}_l^{-1} \mathbf{H}_l \mathbf{x} \right] \qquad (11)
\end{aligned}
$$

where the first two terms represent weighted deviations from measurements and the prior state parameters, respectively, the third the AOT temporal smoothness constraints and the fourth the AOT spectral constraint, with respective uncertainty matrices $\mathbf{S}_a$ and $\mathbf{S}_l$. The two matrices $\mathbf{H}_a$ and $\mathbf{H}_l$, representing respectively the temporal and spectral constraints, can be written as block diagonal

matrices

$$\mathbf{H} = \begin{pmatrix} \mathbf{H}^{\rho_0} & \mathbf{0} & \mathbf{0} & \mathbf{0} & \mathbf{0} \\ \mathbf{0} & \mathbf{H}^{k} & \mathbf{0} & \mathbf{0} & \mathbf{0} \\ \mathbf{0} & \mathbf{0} & \mathbf{H}^{\theta} & \mathbf{0} & \mathbf{0} \\ \mathbf{0} & \mathbf{0} & \mathbf{0} & \mathbf{H}^{\rho_c} & \mathbf{0} \\ \mathbf{0} & \mathbf{0} & \mathbf{0} & \mathbf{0} & \mathbf{H}^{\tau} \end{pmatrix} \tag{12}$$

where the four blocks $\mathbf{H}^{\rho_0}$, $\mathbf{H}^{k}$, $\mathbf{H}^{\theta}$ and $\mathbf{H}^{\rho_c}$ express the spectral constraints between the surface parameters. Their values are set to zero when these constraints are not ~~activated~~active. The submatrix $\mathbf{H}_a^{\tau}$ can also be written using blocks $\mathbf{H}^{\tau}_{a;\tilde{\lambda},v}$ along the diagonal. For a given spectral band $\tilde{\lambda}$ and aerosol ~~vertices~~ vertex $v$, the block $\mathbf{H}^{\tau}_{a;\tilde{\lambda},v}$ is defined as follows

$$\mathbf{H}^{\tau}_{a;\tilde{\lambda},v}\,\boldsymbol{\tau}_{\tilde{\lambda},v} = \begin{pmatrix} 1 & -1 & 0 & \dots & \dots \\ 0 & 1 & -1 & 0 & \dots \\ \dots & \dots & \dots & \dots & \dots \\ \dots & \dots & \dots & 1 & -1 \\ \dots & \dots & \dots & \dots & 0 \end{pmatrix} \begin{pmatrix} \tau_{\tilde{\lambda},v,1} \\ \tau_{\tilde{\lambda},v,2} \\ \vdots \\ \tau_{\tilde{\lambda},v,N_t-1} \\ \tau_{\tilde{\lambda},v,1,N_t} \end{pmatrix} \tag{13}$$

In the same way, the submatrix $\mathbf{H}_l^{\tau}$ can be written using blocks $\mathbf{H}^{\tau}_{l;v,t}$. For a given aerosol vertex $v$ and time $t$, the block $\mathbf{H}^{\tau}_{l;v,t}$ is defined as follows

$$\mathbf{H}^{\tau}_{l;v,t}\,\boldsymbol{\tau}_{v,t} = \begin{pmatrix} 0 & 0 & 0 & \dots & 0 \\ -\frac{\epsilon_2}{\epsilon_1} & 1 & 0 & \dots & 0 \\ 0 & -\frac{\epsilon_3}{\epsilon_2} & 1 & \dots & 0 \\ \dots & \dots & \dots & \ddots & 0 \\ \dots & \dots & \dots & -\frac{\epsilon_{N_\lambda}}{\epsilon_{N_\lambda-1}} & 1 \end{pmatrix} \begin{pmatrix} \tau_{1,v,t} \\ \tau_{2,v,t} \\ \tau_{3,v,t} \\ \vdots \\ \tau_{N_{\tilde{\lambda}},v,t} \end{pmatrix} \tag{14}$$

where the $\epsilon_l$ represents the uncertainties associated with the AOT spectral constraints of the individual vertex $v$ bounding the solution space. The spectral variations of $\tau_v$ between band $\tilde{\lambda}_l$ and $\tilde{\lambda}_{l+1}$ writes

$$\frac{\tau_{\tilde{\lambda}_l,v}}{\tau_{\tilde{\lambda}_{l+1},v}} = \frac{e_{\tilde{\lambda}_l}}{e_{\tilde{\lambda}_{l+1}}} \tag{15}$$

where $e_{\tilde{\lambda}_l}$ the extinction coefficient in band $\tilde{\lambda}_l$.

Maximising the probability function in Equation (11) is equivalent to minimising the negative logarithm

$$J(\mathbf{x}) = J_y(\mathbf{x}) + J_x(\mathbf{x}) + J_a(\mathbf{x}) + J_l(\mathbf{x}) \tag{16}$$

with

$$J_y(\mathbf{x}) = \left(y_m(\mathbf{x},\mathbf{b},\Omega) - \mathbf{y}_{\Omega\tilde{\Lambda}}\right) \mathbf{S}_y^{-1} \left(y_m(\mathbf{x},\mathbf{b},\Omega) - \mathbf{y}_{\Omega\tilde{\Lambda}}\right)^T \tag{17}$$

$$J_x(\mathbf{x}) = \left(\mathbf{x} - \mathbf{x}_b\right) \mathbf{S}_x^{-1} \left(\mathbf{x} - \mathbf{x}_b\right)^T \tag{18}$$

$$J_a(\mathbf{x}) = \mathbf{x}^T\, \mathbf{H}_a^T\, \mathbf{S}_a^{-1}\, \mathbf{H}_a\, \mathbf{x} \tag{19}$$

$$J_l(\mathbf{x}) = \mathbf{x}^T\, \mathbf{H}_l^T\, \mathbf{S}_l^{-1}\, \mathbf{H}_l\, \mathbf{x} \tag{20}$$

Notice that the cost function $J$ is minimized with respect to the state variable $\mathbf{x}$, so that the derivative of $J$ is independent of the model parameters $\mathbf{b}$ which therefore cannot be part of the solution. The need for angular sampling to document the surface anisotropy leads to an unbalanced size of $n_x$ and $n_y$ with $n_y > n_x$ where $n_y$ and $n_x$ represents the number of observations and state variables respectively. According to Dubovik et al. (2006), these additional observations should improve the retrieval as, from a statistical point of view, repeating the same observation implies that the variance of ~~the observation~~ repeated similar observations should decrease. Accordingly, the magnitude of the elements of the covariance matrix should decrease as $1/\sqrt{n_y}$. Thus, repeating similar observations results in some enhancements of retrieval accuracy which should be proportional to the ratio $n_y/n_x$. Hence, the cost function which is actually minimized is ~~$J'(\mathbf{x}) = J_y(\mathbf{x}) + n_y/n_x\,(J_x(\mathbf{x}) + J_a(\mathbf{x}) + J_l(\mathbf{x}))$~~ $J_s(\mathbf{x}) = J_y(\mathbf{x}) + n_y/n_x\,(J_x(\mathbf{x}) + J_a(\mathbf{x}) + J_l(\mathbf{x}))$.

### 5.3 Retrieval uncertainty estimation

The retrieval uncertainty is based on the OE theory, assuming a linear behaviour of $y_m(\mathbf{x},\mathbf{b};\mathbf{m})$ in the vicinity of the solution $\hat{\mathbf{x}}$. Under this condition, the retrieval uncertainty $\sigma_{\hat{\mathbf{x}}}$ is determined by the shape of $J(\mathbf{x})$ ~~in~~ at $\hat{\mathbf{x}}$

$$\sigma^2_{\hat{\mathbf{x}}} = \left( \frac{\partial^2 J(\mathbf{x})}{\partial \mathbf{x}^2} \frac{\partial^2 J_s(\mathbf{x})}{\partial \mathbf{x}^2} \right)^{-1} = \left( \mathbf{K}_x^T \mathbf{S}_y^{-1} \mathbf{K}_x + \mathbf{S}_x^{-1} + \mathbf{H}_a^T \mathbf{S}_a{}^{-1} \mathbf{H}_a + \mathbf{H}_l^T \mathbf{S}_l{}^{-1} \mathbf{H}_l \right)^{-1} \tag{21}$$

where $\mathbf{K}_x$ is Jacobian matrix of $y_m(\mathbf{x},\mathbf{b};\mathbf{m})$ calculated in $\hat{\mathbf{x}}$. Combining Equations (21) and (8), the uncertainty in the retrieval of $\omega_0$ in band $\tilde{\lambda}$ writes

$$\sigma^2_{\hat{\omega}_0}(\tilde{\lambda}) = \sum_v \left( \frac{\omega_{0,v}(\tilde{\lambda}) - \omega_0(\tilde{\lambda})}{\tau_a(\tilde{\lambda})} \right)^2 \sigma^2_{\hat{\tau}_v}(\tilde{\lambda}) \tag{22}$$

A similar equation can be derived for the estimation of $\sigma^2_g$.

### 5.4 Acceleration methods

The minimization of Equation (16) relies on an iterative approach with $y_m(\mathbf{x},\mathbf{b};\mathbf{m})$ and the associated Jacobians $\mathbf{K}_x$ being estimated at each iteration. In order to reduce the calculation time dedicated to the estimation of $y_m(\mathbf{x},\mathbf{b};\mathbf{m})$ and $\mathbf{K}_x$, a series of methods have been implemented ~~to speed-up the execution time~~. All quantities that do not explicitly depend on the state variables ~~such~~ , such as the observation conditions $\mathbf{m}$, model parameters $\mathbf{b}$, quadrature point weight, *etc*, are computed only once prior to the optimization.

When solving the RTE, the estimation of the multiple scattering term is by far the most time-consuming step. Hence, during the iterative optimisation process, when the change $\Delta\tau_a(\tilde{\lambda})$ of $\tau_a(\tilde{\lambda})$ between iteration $j$ and $j+1$ is small, the multiple scattering contribution at iteration $j+1$ is estimated with

$$I^{\uparrow}_m(\tau_a(j+1,\tilde{\lambda}),\mathbf{b};\mathbf{m}) = I^{\uparrow}_m(\tau_a(j,\tilde{\lambda}),\mathbf{b};\mathbf{m}) + \frac{\partial I^{\uparrow}_m(\tau_a(j,\tilde{\lambda}),\mathbf{b};\mathbf{m})}{\partial \tau_a} \Delta\tau_a(\tilde{\lambda}) \tag{23}$$

This approximation is not used twice consecutively to avoid inaccurate results, and the single scattering contribution is always explicitly estimated.

**Table 2.** List of aerosol properties used for the simulations. The parameters $r_{mf}$ and $r_{mc}$ are the median fine and coarse mode radii expressed in $\mu$m. Their respective standard deviations are $\sigma_{r_{mf}}$ and $\sigma_{r_{mc}}$. The parameters $n_r$ and $n_i$ are the real and imaginary part of the refractive index in the indicated bands. $N_f$ and $N_c$ are the fine and coarse mode particle concentration in number of particles per cm$^3$. ~~Wavelengths are given in .~~

| Centre band in $\mu$m | | | 0.44 | 0.55 | 0.67 | 0.87 | | |
|---|---|---|---|---|---|---|---|---|
| F0 | 0.08 | - | 1.3958 | 1.3932 | 1.3909 | 1.3879 | - | - |
| F1 | 0.10 | 0.93 | 1.4189 | 1.4269 | 1.4357 | 1.4417 | 9.587 | 0.002 |
| F2 | 0.08 | 0.77 | 1.4985 | 1.5201 | 1.5436 | 1.5417 | 8.975 | 0.024 |
| | $\sigma_{r_{mf}}$ | $\sigma_{r_{mc}}$ | $n_i$ | $n_i$ | $n_i$ | $n_i$ | | |
| F0 | 0.45 | - | 0.0123 | 0.0123 | 0.0122 | 0.0121 | - | - |
| F1 | 0.43 | 0.62 | 0.0057 | 0.0055 | 0.0053 | 0.0051 | | |
| F2 | 0.50 | 0.62 | 0.0054 | 0.0047 | 0.0040 | 0.0036 | | |

## 6 Algorithm performance evaluation

### 6.1 Experimental setup

A simple experimental setup based on simulated data has been defined to illustrate the behaviour of the CISAR algorithm as a function of the delineated solution space. More specifically, its capability to continuously sample the $[g,\omega_0]$ solution space is examined in detail. For the sake of simplicity, a noise-free multi-angular observation vector $\mathbf{y}_{\Omega\tilde{\Lambda}}$, where $\Omega$ expresses the illumination and viewing geometries, is assumed to be acquired instantaneously in the principal plane and in the spectral bands listed in Table (1). An uncertainty of 3% is assumed in matrix $\mathbf{S}_y$. In this ideal configuration, the Sun Zenith Angle (SZA) is set to 30°. It is also assumed that the surface parameters are known a priori with zero bias and an uncertainty of 0.03 for each RPV parameter, though these parameters are allowed to vary. Such assumption can be justified applying the method and associated results described in Wagner et al. (2010). No prior information is assumed for the aerosol optical thickness, *i.e.*, the prior uncertainty is set to very large values. Only regularization on the spectral variations of $\tau_a$ is applied.

The CISAR algorithm performance evaluation is based on a series of experiments corresponding to different selections of aerosol properties, both for the forward simulation of the observations and their inversion. Three different aerosol models are used in the forward simulations: F0 which only contains small particles, F1 which contains a dual-mode particle size distribution dominated by small particles, and F2 composed of a dual-mode distribution dominated by the coarse particles. Table (2) contains the values of the size distribution and refractive indices of these aerosol classes.

**Table 3.** Micro-physical parameter values for the four FA, FN, CS, CL vertices in the selected spectral bands. Radius ~~and wavelengths~~ are given in $\mu$m

| Centre band in $\mu$m | | | 0.44 | 0.55 | 0.67 | 0.87 | 0.44 | 0.55 | 0.67 | 0.87 |
|---|---|---|---|---|---|---|---|---|---|---|
| Type | $r_m$ | $\sigma_{r_m}$ | $n_r$ | $n_r$ | $n_r$ | $n_r$ | $n_i$ | $n_i$ | $n_i$ | $n_i$ |
| FN | 0.08 | 0.45 | 1.3958 | 1.3932 | 1.3909 | 1.3879 | 0.0006 | 0.0006 | 0.0006 | 0.0006 |
| FA | 0.08 | 0.45 | 1.3958 | 1.3932 | 1.3909 | 1.3879 | 0.0207 | 0.0207 | 0.0207 | 0.0205 |
| CS | 0.30 | 0.55 | 1.4889 | 1.4878 | 1.4845 | 1.4763 | 0.0029 | 0.0029 | 0.0029 | 0.0029 |
| CL | 1.00 | 0.55 | 1.4889 | 1.4878 | 1.4845 | 1.4763 | 0.0029 | 0.0029 | 0.0029 | 0.0029 |

Corresponding values for the four FA, FN, CL, CS vertices enclosing the solution space as illustrated ~~on~~ in Fig. (??3) are given in Table (3). When the observations simulated with aerosol types F0, F1 or F2 are inverted, the list of vertices actually used depends on the type of experiments indicated in Table (4). The objective of these experiments is to illustrate the impact of the ~~solution space delineation~~ selected solution space on the retrieved aerosol properties. For all these scenarios, an AOT of 0.4 at 0.55$\mu$m is assumed.

**Table 4.** List of experiments the name of which is provided in the first column. The active vertices in each experiments are indicated with the $\times$ symbol. The last column indicates the name of the aerosol model used to simulate the observations.

| Exp. | Active vertices | | | | Forward type |
|---|---|---|---|---|---|
| | FA | FN | CS | CL | |
| F00 | $\times$ | $\times$ | | | F0 |
| F10 | $\times$ | $\times$ | | | F1 |
| F11 | $\times$ | $\times$ | $\times$ | | F1 |
| F12 | $\times$ | $\times$ | | $\times$ | F1 |
| F13 | $\times$ | $\times$ | $\times$ | $\times$ | F1 |
| F21 | $\times$ | $\times$ | $\times$ | | F2 |
| F22 | $\times$ | $\times$ | | $\times$ | F2 |
| F23 | $\times$ | $\times$ | $\times$ | $\times$ | F2 |

**Table 5.** Values of the surface RPV parameters as used in the experiments for the prior information. Wavelengths are given in $\mu$m.

| Wavelength | $\rho_0$ | $k$ | $\Theta$ | $\rho_c$ |
|---|---|---|---|---|
| 0.44 | 0.025 | 0.666 | -0.150 | 0.125 |
| 0.55 | 0.047 | 0.657 | -0.114 | 0.023 |
| 0.67 | 0.056 | 0.710 | -0.096 | 0.025 |
| 0.87 | 0.238 | 0.706 | -0.019 | 0.030 |

Values used for the RPV parameters in the four selected bands are indicated in Table (5). They correspond to typical BRF values that would be observed over a vegetated surface with a leaf area index value of 3 and a bright underling soil.

The primary objective of these experiments is to illustrate the behaviour of the proposed algorithm as a function of the selected vertices. It is therefore not intended to demonstrate that the algorithm can work in all possible conditions. Examples of retrieval against actual satellite observations can be found in Luffarelli et al. (2016).

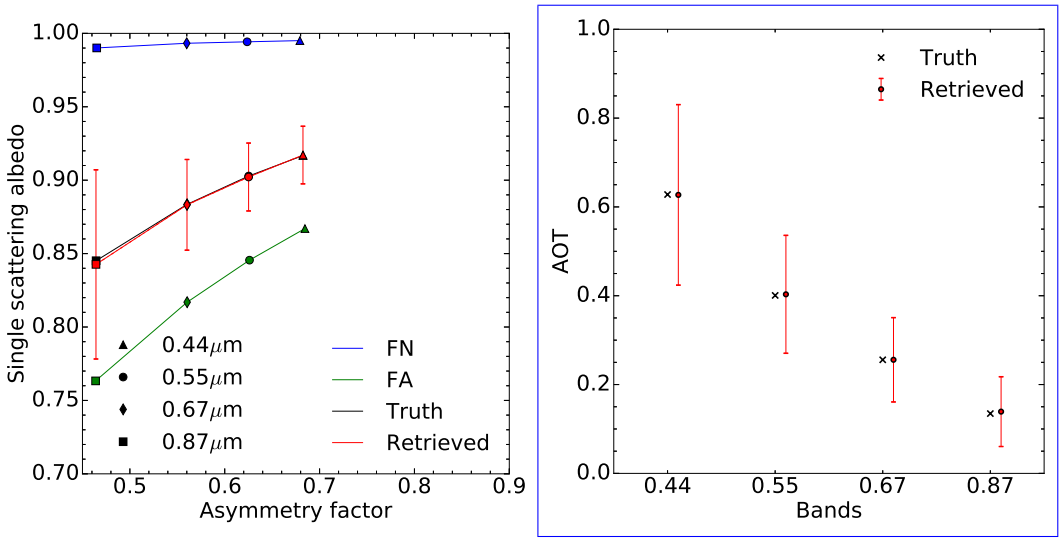


**Fig. 5. Left panel**: Results of experiment F00 in the $[g,\omega_0]$ space. ~~Aerosol~~ The aerosol vertices used for the inversion are FN (blue) and FA (green). The forward aerosol properties are shown in black and the retrieved ones in red. Vertical and horizontal red bars indicate the uncertainty, if any, of the retrieved values. ~~The four processed wavelengths are indicated with the following symbols: 0.44(triangle), 0.55(circle), 0.67(diamond), 0.87(square).~~ **Right panel**: Retrieved AOT in the four processed spectral bands (red circles). The retrieval uncertainty is shown with the vertical red lines. True values are indicated with black crosses.

## 6.2 Results

### 6.2.1 Experiment F00

The purpose of the first experiment (F00) is to demonstrate that the CISAR algorithm can accurately retrieve aerosol properties in a simple situation, showing ~~thereby~~ therefore that the inversion process works correctly. The F0 aerosol class used to simulate the observations is only composed of fine particles with a median radius of 0.08$\mu$m, *i.e.*, the same value as for the FN and FA vertices used for the inversion. Hence, only the imaginary part of the index of refraction differs from the ~~ones~~ values used for the generation of these two vertices, the real part being set to 1.4. With such a retrieval configuration restricted to the use of only two vertices, the solution space for each wavelength is

~~actually~~ limited to a straight line between the two vertices.

Results are shown in Fig. (5) for the atmosphere and Table (6) for the surface. The asymmetry factor $g$ and single scattering albedo $\omega_0$ are almost exactly retrieved. There is practically no uncertainty in the retrieval of $g$ because of the constraints imposed by the fact that the particle radius is the same as for the F0 aerosol class. The estimated single scattering albedo uncertainty is much larger than the asymmetry one, though the retrieved values match exactly the true ones. The retrieved AOT is also in very good agreement with the true values as can be seen on the right panel in Fig. (5). To further evaluate the performance of the CISAR algorithm, the retrieval error $\epsilon_\tau$ is defined as the ~~straight~~ difference between the retrieved and the true AOT values. Results are summarised in Table (7). This first experiment demonstrates that it is possible to retrieve the properties of the aerosol class F0 as a linear combination of the vertices FA and FN when only the absorption varies, the particle median radius being ~~kept~~ constant.

A comparison between Tables (5) and (6) shows that the surface parameters are very accurately retrieved. As stated in Section (6.1), prior information on the magnitude of the RPV parameter is assumed unbiased with an uncertainty of 0.03. The corresponding posterior uncertainties exhibit a significant decrease for the $\rho_0$ parameter ~~in~~ at all wavelengths. A similar behaviour is not observed for the other parameters. As explained in Wagner et al. (2010), the $k$ and $\Theta$ parameters, controlling the surface reflectance anisotropy, are strongly correlated with ~~the~~ amount atmospheric scattering. Consequently, the retrieved uncertainties decrease with the wavelengths, *i.e.*, as a function of the actual AOT. Despite the observations are taking place in the principal plane, the posterior uncertainty on the hot spot parameter remains equal to the prior one as a result of atmospheric scattering. ~~In other words, this parameter can only be retrieved when the optical thickness is very low~~This fact is attributed to the relatively high value of the true AOT, and the consequent amount of scattering able to attenuate the hot spot effects. Results for the surface parameter retrieval exhibits a very similar behaviour for the other experiments and will not be shown.

**Table 6.** Values of the retrieved surface RPV parameters and associated uncertainties for experiment F00. Wavelengths are given in $\mu$m.

| | Value | | | | Uncertainty | | | |
|---|---|---|---|---|---|---|---|---|
| Band | $\rho_0$ | $k$ | $\Theta$ | $\rho_c$ | $\rho_0$ | $k$ | $\Theta$ | $\rho_c$ |
| | Posterior | | | | | | | |
| 0.44 | 0.025 | 0.666 | -0.150 | 0.125 | 0.006 | 0.030 | 0.030 | 0.030 |
| 0.55 | 0.047 | 0.657 | -0.116 | 0.023 | 0.004 | 0.029 | 0.028 | 0.030 |
| 0.67 | 0.056 | 0.711 | -0.096 | 0.025 | 0.004 | 0.028 | 0.026 | 0.030 |
| 0.87 | 0.238 | 0.705 | -0.020 | 0.029 | 0.011 | 0.025 | 0.017 | 0.030 |

### 6.2.2 Experiment F10

Let us now examine the case where both the $r_m$ and $n_i$ used to describe the forward aerosol properties differ from those of the vertices used for the inversion. For that purpose, aerosol type F1 is used for the forward simulation with ~~$r_{mf} = 0.1\mu m$~~ $r_{mf} = 0.1\mu$m for the predominant fine mode and ~~$r_{mc} = 0.93\mu m$~~ $r_{mc} = 0.93\mu$m for the coarse mode. The same aerosol vertices as in experiments F00 are used for the inversion.

The results in Fig. (6) show that $\omega_0$ is reasonably well retrieved unlike the $g$ parameter, which is systematically underestimated. At any given wavelengths, it is not possible to retrieve $g$ values outside the bounds defined by the FA and FN vertices. Consequently, the retrieved AOT values are underestimated by about 10% (Table 7). Additionally, the estimated error on $g$ is largely underestimated. This example illustrates the ~~erroneous behaviour of CISAR~~ retrieval failure when the actual solution lays outside the $[g,\omega_0]$ space defined by the active vertices.

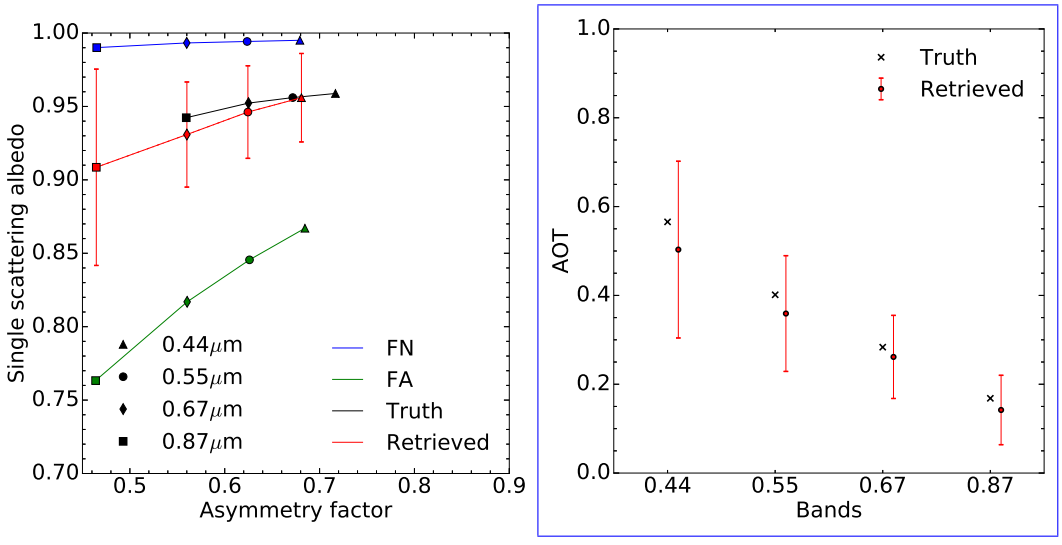


**Fig. 6.** Same as Fig. (5) but for experiment F10.

### 6.2.3 Experiments F11 - F13

In order to improve the retrieval of the F1 aerosol class properties, the additional aerosol CS vertex has been added in layer $L_a$ during the inversion process, *i.e.*, a coarse mode with ~~$r_m = 0.3\mu m$~~ $r_m = 0.3\mu$m. Results of experiment F11 are displayed on Fig. (7). Retrieved $g$ values are no longer systematically underestimated. The single scattering albedo is slightly underestimated. It should be noted that the estimated uncertainty associated with $g$ increases with wavelength and is particularly large at $0.87\mu$m, but rather underestimated at $0.44\mu$m. The improvement in the AOT retrieval accuracy is noticeable in the $0.44\mu$m and $0.55\mu$m bands where the magnitude of $\epsilon_r$ is reduced from 0.062 to 0.005 and from 0.042 to -0.021 respectively (Table 7). At larger wavelengths,

**Table 7.** Retrieved AOT error and uncertainties for the six experiments in the four processed bands. The $\epsilon_\tau$ symbol is the error calculated as the difference between the retrieved value and the truth, $\delta_\tau$ the relative error in percent and $\sigma_\tau$ the retrieval uncertainty estimated with Equation (21).

| BAND | 0.44 | | | 0.55 | | | 0.67 | | | 0.87 | | |
|---|---|---|---|---|---|---|---|---|---|---|---|---|
| EXP | $\epsilon_\tau$ | $\delta_\tau$ (%) | $\sigma_\tau$ | $\epsilon_\tau$ | $\delta_\tau$ (%) | $\sigma_\tau$ | $\epsilon_\tau$ | $\delta_\tau$ (%) | $\sigma_\tau$ | $\epsilon_\tau$ | $\delta_\tau$ (%) | $\sigma_\tau$ |
| F00 | 0.001 | -0.1 | 0.203 | -0.002 | 0.6 | 0.133 | -0.000 | 0.0 | 0.095 | -0.004 | 3.3 | 0.079 |
| F10 | 0.062 | -11.0 | 0.199 | 0.042 | -10.5 | 0.130 | 0.022 | -7.8 | 0.094 | 0.026 | -15.6 | 0.078 |
| F11 | 0.005 | -0.9 | 0.239 | -0.021 | 5.3 | 0.164 | -0.037 | 13.2 | 0.125 | -0.047 | 27.8 | 0.095 |
| F12 | 0.041 | -7.3 | 0.228 | 0.013 | -3.3 | 0.152 | -0.004 | 1.5 | 0.113 | -0.015 | 8.6 | 0.089 |
| F13 | -0.001 | 0.1 | 0.295 | -0.028 | 6.9 | 0.199 | -0.041 | 14.5 | 0.145 | -0.051 | 30.5 | 0.103 |
| F21 | 0.018 | -3.9 | 0.252 | 0.037 | -9.2 | 0.172 | 0.042 | -11.9 | 0.129 | 0.071 | -22.9 | 0.096 |
| F22 | -0.018 | 3.9 | 0.236 | -0.007 | 1.8 | 0.158 | -0.004 | 1.1 | 0.116 | 0.008 | -2.6 | 0.090 |
| F23 | -0.041 | 8.8 | 0.296 | -0.031 | 7.8 | 0.200 | -0.027 | 7.5 | 0.145 | -0.018 | 6.0 | 0.103 |

the benefit of adding the CS ~~vertices~~ vertex is less noticeable though the magnitude of $\epsilon_r$ remains below 0.05. Finally, the retrieval uncertainty slightly increases ~~with the use of an additional CS vertices~~ from 0.199 up to 0.239 in the 0.44$\mu$m band because of the use of additional state variables $\tau_v$ associated with ~~that~~ the inclusion of an additional vertex.

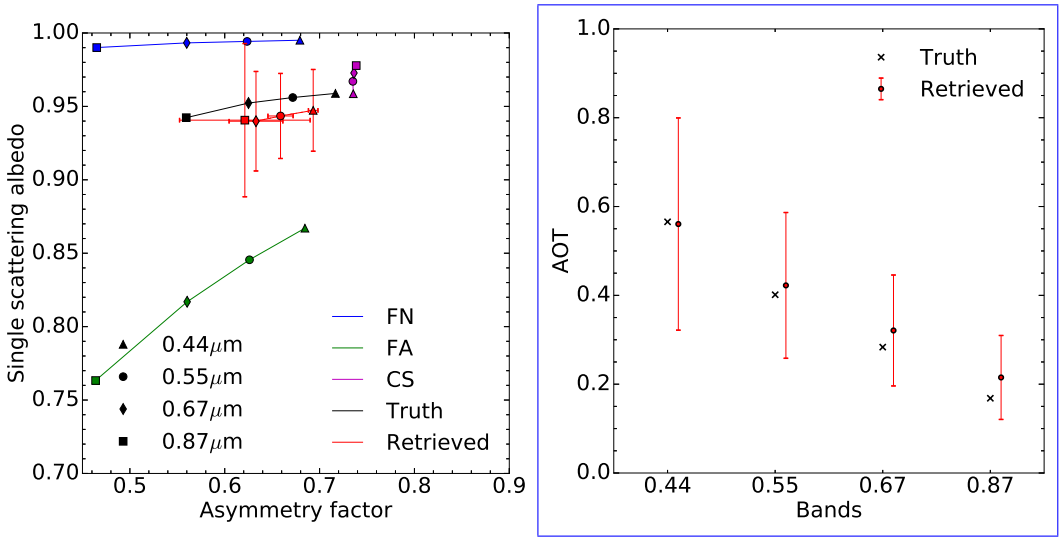


**Fig. 7.** Same as Fig. (5) but for experiment F11.

For experiment F12, the CS vertex is substituted by vertex CL which has a median radius of 1.0$\mu$m. ~~As can be seen in Fig. (8), the~~ The use of this vertex instead of CS considerably improves the retrieval of $g$ and of $\omega_0$ at large wavelengths ~~.~~ (Fig. 8). As can be seen in Fig. (2), the sensitivity of aerosol single scattering properties to particle median radius and imaginary part of the refractive

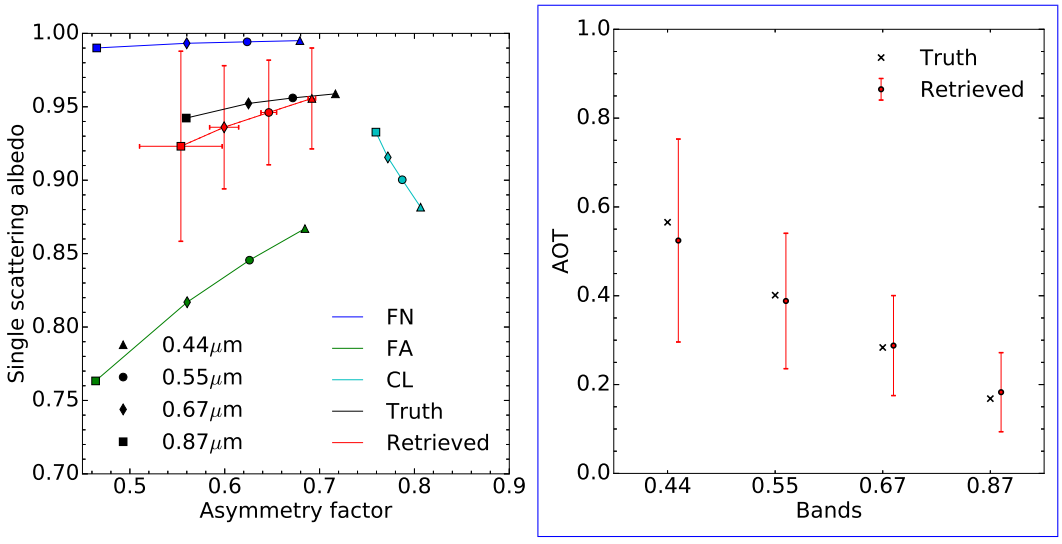


**Fig. 8.** Same as Fig. (5) but for experiment F12.

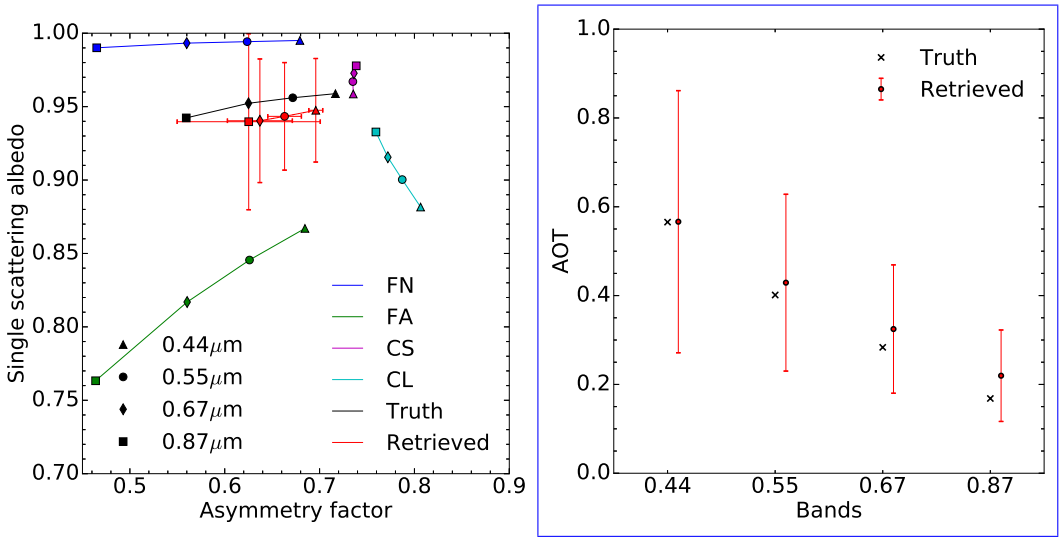


**Fig. 9.** Same as Fig. (5) but for experiment F13.

index depends on the ~~wavelengths~~wavelength. Hence, a similar behaviour of the algorithm in all wavelengths should not be expected. The errors $\epsilon_\tau$ ~~is~~ in this experiment F12 are further reduced ~~with respect~~ compared to experiment F11 with the exception of the 0.44$\mu$m band. The CISAR algorithm manages ~~however~~ to correctly retrieve the total AOT.

Finally, the inversion has been performed using all four vertices (Fig. 9) in experiment F13. ~~The~~ This additional degree of freedom translates into ~~a significant~~ an increase of the estimated uncertainty $\sigma_{\hat{\tau}}$ as a result of the large number of possible way to combine these four vertices to retrieve the properties of the aerosol class F1. In other words, adding two coarse mode vertices does not improve the characterization of F1. The actual benefit of adding this fourth vertex is therefore not

straightforward~~. It~~, and should be noted that increasing the number of vertices impacts the computational time. This series of simple three experiments has shown that the use of the FN, FA and CL vertices provides the best combination for the retrieval of the properties of aerosol class F1. With this combination, the FN and FA vertices allow to control the amount of radiation absorbed by the aerosols and the CL vertex the effects of the particle size.

### 6.2.4 Experiments F21 - F23

The retrieval of aerosol class F2, a dual mode particle size distribution dominated by coarse particles, is now examined. This class is composed of a fine mode radius $r_{mf}$ of 0.08$\mu$m and coarse mode one $r_{mc}$ of 0.77$\mu$m. As for the retrieval of the F1 aerosol class, three combinations of vertices have been explored, *i.e.*, (FN, FA, CS) for experiment F21 (Fig. 10), (FN, FA, CL) for experiment F23 (Fig. 11) and finally (FN, FA, CS, CL) for experiment F22 (Fig. 11). Essentially the same conclusions hold as for the retrieval of aerosol class F1. The retrieval of ~~F2 class~~ F2-class properties expressed as a linear combination of the (FN, FA, CL) vertices provides the best solution. Values of both $g$ and $\omega_0$ are well retrieved at all wavelengths.

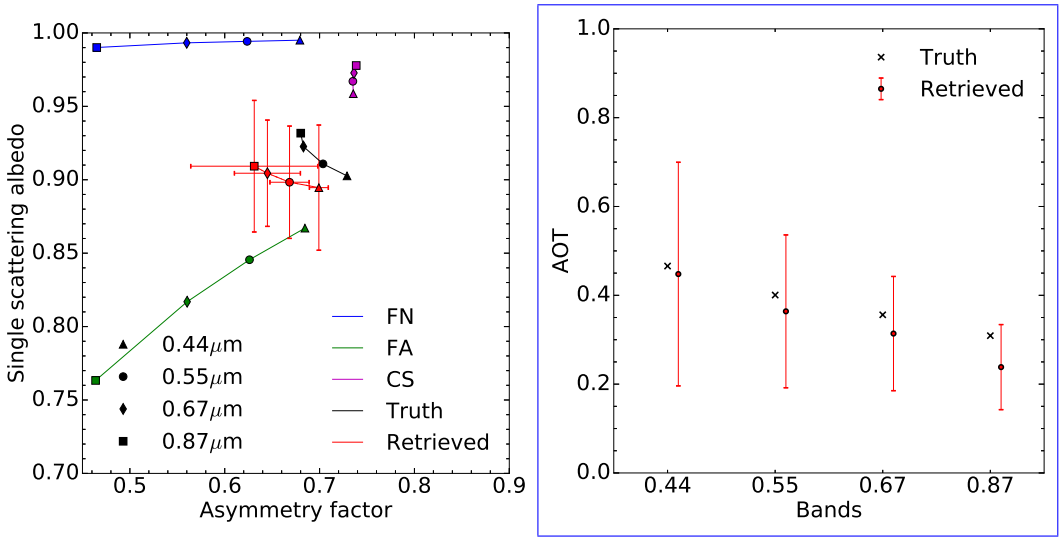


**Fig. 10.** Same as Fig. (5) but for experiment F21.

## 7 Discussion and conclusion

This paper describes the CISAR algorithm designed for the joint retrieval of surface reflectance and aerosol properties. Previous attempts to perform such joint retrieval have been reviewed, discussing their advantages and weaknesses. That analysis revealed that retrieval methods based on OE applied only to a limited number of aerosol classes represent a major drawback as it does not permit a continuous variation of the state variables in the solution space. The new method presented in this paper

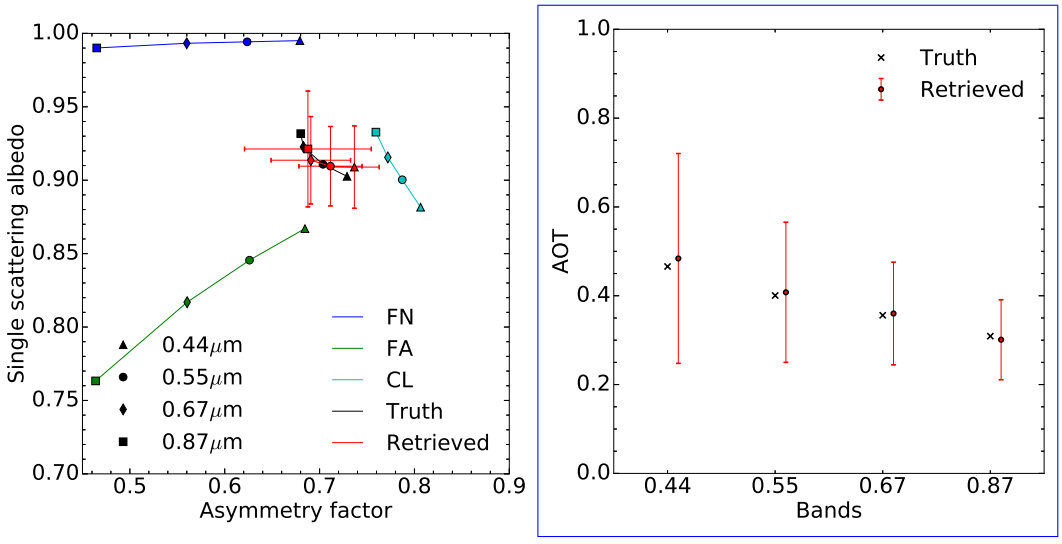


**Fig. 11.** Same as Fig. (5) but for experiment F22.

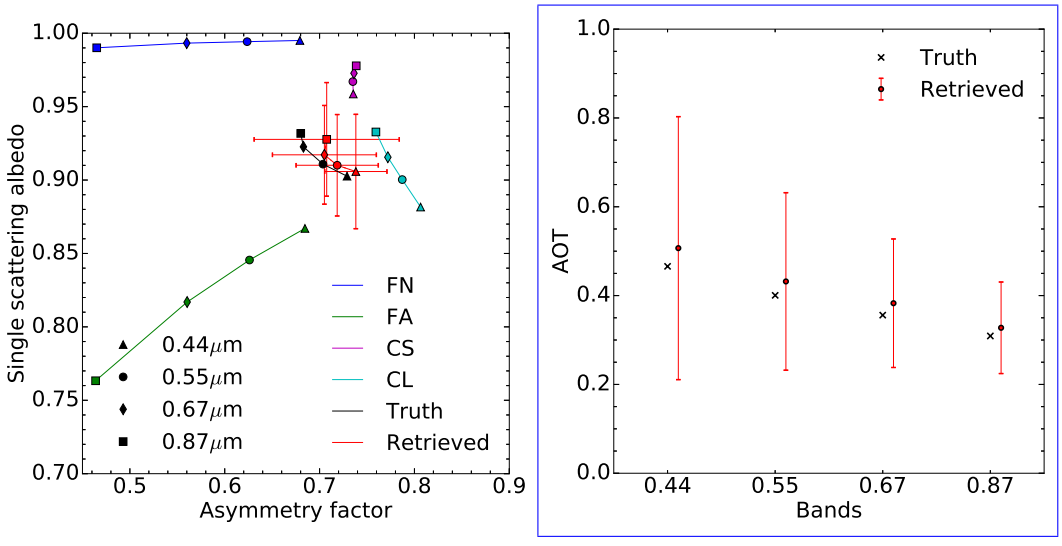


**Fig. 12.** Same as Fig. (5) but for experiment F23.

specifically addresses this issue, allowing ~~a~~ continuous variations of the aerosol single scattering properties in the solution space without having the ~~parameters describing the~~ aerosol micro-physical properties explicitly appearing as state variables.

A fast forward radiative transfer model has been designed for this purpose, which solves the radiative transfer equation without relying on pre-computed look-up tables. This model considers only two layers in the atmosphere. The upper layer only hosts molecular absorption. The lower layer accounts for both absorption and scattering processes due to aerosols and molecules and is radiative coupled with the surface represented with the RPV BRF model. Single scattering aerosol properties in this layer are expressed as a linear combination of the properties of vertices enclosing the solution

space.

A series of different experiments has been ~~defined~~ devised to analyse the behaviour of the CISAR algorithm and its capability to retrieve aerosol single scattering properties as well as optical thickness. This discussion focuses on the retrieval of aerosol classes F1 dominated by the fine mode and F2 dominated by the coarse mode. These two classes have pretty different spectral behaviour in the $[g,\omega_0]$ space and yet the CISAR algorithm is capable of retrieving the corresponding single scattering properties in both cases.

These experiments illustrate the possibility to use Equations (8) and (9) for the continuous retrieval of the aerosol single scattering albedo and phase function properties in the solution space. These equations assume a linear behaviour of $\omega_0$ and $g$ in the solution space illustrated in Fig. (~~??~~3) as a function of the variations of the aerosol micro-physical properties. Such assumptions have proven to be valid for the case addressed in experiment F00. This assumption is not exactly true for the retrieval of more realistic aerosol classes composed of a fine and a coarse participle size modes. However, the retrieved aerosol single scattering properties are derived much more accurately than with a method based on a limited number of predefined aerosol classes as in Govaerts et al. (2010) where only the single scattering properties of the predefined classes can be exactly retrieved. It thus represents a major improvement with respect to these type of retrieval approaches without requiring the use of a large number of state variables as in the method proposed by Dubovik et al. (2011), where aerosol micro-physical properties are explicitly included in the set of retrieved state variables. ~~The CISAR algorithm is thus suited for the retrieval of aerosol properties over land from space-based imagers which provide a limited number of independent observations.~~

The choice of the vertices outlining the $[g,\omega_0]$ solution space is critical. In these experiments, best retrieval is obtained using three vertices, *i.e.*, one vertex composed of small weakly absorbing particles (FN), one vertex composed of small absorbing particles (FA) and one vertex composed of large particles (CL). The use of a fourth vertex (CS) does not improve the retrieval and increases the estimated retrieval uncertainty.

This set of experiments represents ideal conditions, *i.e.*, noise-free observations in the principal plane with no bias on the surface prior. This choice is motivated by the need to keep the result interpretation simple, the primary objective being to illustrate how the new retrieval concept developed in this paper works. These experiments show the possibility to retrieve aerosol single scattering ~~property~~ properties within the solution space provided it is correctly bounded by the vertices. It is clear that adding noise in the observations will degrade the quality of the retrieval. Similar conclusions can hold in case the ~~angular observations are~~ observations are taking place far from the principal plane where most of the angular variations occur. It should be stressed that this approach can also be applied for the retrieval of similar properties within a single cloud layer or a mixture of cloud and aerosol.

Such an algorithm therefore represents a decisive improvement with respect to the method pro-

posed by Govaerts et al. (2010) which retrieves the aerosol optical thickness only for the very limited number of pre-defined aerosol classes. The CISAR algorithm allows a continuous variation of the aerosol single scattering properties adding only a limited number of state variables, *i.e.*, the optical thickness of each vertices.

## 8 Acknowledgements

*Acknowledgements.* The authors would like to thanks the reviewers for their fruitful suggestions.

## References


Cox, C. and Munk, W.: Measurement of the Roughness of the Sea Surface from Photographs of the Sun's Glitter, Journal of the Optical Society of America, 44, 838–850, doi:10.1364/JOSA.44.000838, 1954.

Diner, D. J., Hodos, R. A., Davis, A. B., Garay, M. J., Martonchik, J. V., Sanghavi, S. V., von Allmen, P., Kokhanovsky, A. A., and Zhai, P.: An optimization approach for aerosol retrievals using simulated MISR radiances, Atmospheric Research, 116, 1–14, doi:10.1016/j.atmosres.2011.05.020, 2012.

Dubovik, O., Sinyuk, A., Lapyonok, T., Holben, B. N., Mishchenko, M., Yang, P., Eck, T. F., Volten, H., Munoz, O., Veihelmann, B., van der Zande, W. J., Leon, J. F., Sorokin, M., and Slutsker, I.: Application of spheroid models to account for aerosol particle nonsphericity in remote sensing of desert dust, Journal of Geophysical Research-Atmospheres, 111, 11 208–11 208, 2006.

Dubovik, O., Herman, M., Holdak, A., Lapyonok, T., Tanr, D., Deuz, J. L., Ducos, F., Sinyuk, A., and Lopatin, A.: Statistically optimized inversion algorithm for enhanced retrieval of aerosol properties from spectral multi-angle polarimetric satellite observations, Atmospheric Measurement Techniques, 4, 975–1018, 2011.

Fischer, J. and Grassl, H.: Radiative transfer in an atmosphere-ocean system: an azimuthally dependent matrix-operator approach, Applied Optics, 23, 1032–1039, 1984.

Govaerts, Y. and Lattanzio, A.: Retrieval Error Estimation of Surface Albedo Derived from Geostationary Large Band Satellite Observations: Application to Meteosat-2 and -7 Data, Journal of Geophysical Research, 112, doi:10.1029/2006JD007 313, 2007.

Govaerts, Y., Luffarelli, M., and Damman, A.: Effects of Sky Radiation on Surface Reflectance: Implications on The Derivation of LER from BRF for the Processing of Sentinel-4 Observations, in: Living Planet Symposium 2016, Prague, Czech Republic, Prague, Czech Republic, 2016.

Govaerts, Y. M.: RTMOM V0B.10 User's Manual, 2006.

Govaerts, Y. M., Lattanzio, A., Taberner, M., and Pinty, B.: Generating global surface albedo products from multiple geostationary satellites, Remote Sensing of Environment, 112, 2804–2816, doi:10.1016/j.rse.2008.01.012, http://www.sciencedirect.com/science/article/pii/S0034425708000412, 2008.

Govaerts, Y. M., Wagner, S., Lattanzio, A., and Watts, P.: Joint retrieval of surface reflectance and aerosol optical depth from MSG/SEVIRI observations with an optimal estimation approach: 1. Theory, Journal of Geophysical Research, 115, doi:10.1029/2009JD011 779, 2010.

Hess, M., Koepke, P., and Schult, I.: Optical properties of aerosols and clouds: The software package OPAC, Bulletin of the American Meteorological Society, 79, 831–844, 1998.

Kokhanovsky, A. A., Deuz, J. L., Diner, D. J., Dubovik, O., Ducos, F., Emde, C., Garay, M. J., Grainger, R. G., Heckel, A., Herman, M., Katsev, I. L., Keller, J., Levy, R., North, P. R. J., Prikhach, A. S., Rozanov, V. V., Sayer, A. M., Ota, Y., Tanr, D., Thomas, G. E., and Zege, E. P.: The inter-comparison of major satellite aerosol retrieval algorithms using simulated intensity and polarization characteristics of reflected light, Atmos. Meas. Tech., 3, 909–932, doi:10.5194/amt-3-909-2010, 2010.

Lattanzio, A., Schulz, J., Matthews, J., Okuyama, A., Theodore, B., Bates, J. J., Knapp, K. R., Kosaka, Y., and Schller, L.: Land Surface Albedo from Geostationary Satelites: A Multiagency Collaboration within SCOPE-CM, Bulletin of the American Meteorological Society, 94, 205–214, doi:10.1175/BAMS-D-11-00230.1, 2013.

Liu, Q. and Ruprecht, E.: Radiative transfer model: matrix operator method, Applied Optics, 35, 4229–4237,

1996.

Luffarelli, M., Govaerts, Y., and Damman, A.: Assessing hourly aerosol properties retrieval from MSG/SEVIRI observations in the framework of aeroosl-cci2, in: Living Planet Symposium 2016, Prague, Czech Republic, Prague, Czech Republic, 2016.

Luffarelli, M., Govaerts, Y., Goossens, C., Wolters, E., and Swinnen, E.: Joint retrieval of surface reflectance and aerosol properties from PROBA-V observations, part I: algorithm performance evaluation, in: Proceedings of MultiTemp 2017, Bruges, Belgium, 2017.

Manolis, I., Grabarnik, S., Caron, J., Bzy, J.-L., Loiselet, M., Betto, M., Barr, H., Mason, G., and Meynart, R.: The MetOp second generation 3MI instrument, p. 88890J, doi:10.1117/12.2028662, 2013.

Marquardt, D.: An Algorithm for Least-Squares Estimation of Nonlinear Parameters, SIAM Journal on Applied Mathematics, 11, 431–441, 1963.

Pinty, B., Roveda, F., Verstraete, M. M., Gobron, N., Govaerts, Y., Martonchik, J. V., Diner, D. J., and Kahn, R. A.: Surface albedo retrieval from Meteosat: Part 1: Theory, Journal of Geophysical Research, 105, 18 099–18 112, 2000a.

Pinty, B., Roveda, F., Verstraete, M. M., Gobron, N., Govaerts, Y., Martonchik, J. V., Diner, D. J., and Kahn, R. A.: Surface albedo retrieval from Meteosat: Part 2: Applications, Journal of Geophysical Research, 105, 18 113–18 134, 2000b.

Rahman, H., Pinty, B., and Verstraete, M. M.: Coupled surface-atmosphere reflectance (CSAR) model. 2. Semiempirical surface model usable with NOAA Advanced Very High Resolution Radiometer Data, Journal of Geophysical Research, 98, 20,791–20,801, 1993.

Rodgers, C. D.: Inverse methods for atmospheric sounding, Series on Atmospheric Oceanic and Planetary Physics, World Scientific, 2000.

Schuster, G. L., Dubovik, O., Holben, B. N., and Clothiaux, E. E.: Inferring black carbon content and specific absorption from Aerosol Robotic Network (AERONET) aerosol retrievals, Journal of Geophysical Research, 110, S1017–S1017, 2005.

Serene, F. and Corcoral, N.: PARASOL and CALIPSO : Experience Feedback on Operations of Micro and Small Satellites, in: SpaceOps 2006 Conference, American Institute of Aeronautics and Astronautics, dOI: 10.2514/6.2006-5919, 2006.

Vermote, E. F., Tanré, D., Deuzé, J. L., Herman, M., and Morcrette, J. J.: Second simulation of the satellite signal in the solar spectrum, 6S: An overview, IEEE TGARS, 35, 675–686, 1997.

Wagner, S. C., Govaerts, Y. M., and Lattanzio, A.: Joint retrieval of surface reflectance and aerosol optical depth from MSG/SEVIRI observations with an optimal estimation approach: 2. Implementation and evaluation, Journal of Geophysical Research, 115, doi:10.1029/2009JD011 780, 2010.

Wiscombe, W. J.: The Delta-M Method: Rapid Yet Accurate Radiative Flux Calculations for Strongly Asymmetric Phase Functions, Journal of Atmospheric Sciences, 34, 1408–1422, 1977.